Journal of Energy Storage 73 (2023) 109172

Contents lists available at ScienceDirect

Journal of Energy Storage

journal homepage: www.elsevier.com/locate/est

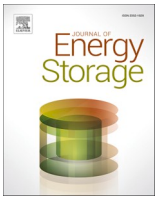

Research papers

Probabilistic sizing and scheduling co-optimisation of hybrid battery/super-capacitor energy storage systems in micro-grids

Soheil Mohseni [a,b,*], Alan C. Brent [a,c]

[a] Sustainable Energy Systems, Faculty of Engineering, Victoria University of Wellington, Wellington 6140, New Zealand
[b] University of Technology Sydney, Institute for Sustainable Futures, Sydney, NSW, 2007, Australia
[c] Department of Industrial Engineering, Centre for Renewable and Sustainable Energy Studies, Stellenbosch University, Stellenbosch 7600, South Africa

ARTICLE INFO

Keywords:
Battery
Super-capacitor
Uncertainty
Co-optimization
Micro-grid
Degradation

ABSTRACT

While established deterministic capacity planning models for single-component energy storage systems exist, little attention has been given to probabilistic sizing of hybrid energy storage systems (ESSs) using swarm-based meta-heuristic algorithms. This highlights two key research opportunities, namely: (1) studying the impact of preserving model-inherent characteristics and optimising daily system dispatch on narrowing reality gaps in hybrid ESS designs, and (2) the optimal integration of hybrid ESSs into grid-connected micro-grids based on their applications, with potentially significant financial implications for model designs. In response, this paper introduces a novel probabilistic hybrid ESS capacity planning optimisation model based on a state-of-the-art meta-heuristic algorithm. To demonstrate the effectiveness of the model within a community micro-grid scheme, a case study of an eco-village in Aotearoa New Zealand is presented. The simulation results indicate a ~4 % and ~36 % premium above the deterministic results respectively in the most likely case and worst-case probabilistic scenarios. On the other hand, the best-case stochastic estimate of the life-cycle cost of the hybrid ESS is found to be ~39 % lower than that of the deterministic modelling. Additionally, the economics of temporal energy arbitrage using the battery bank is investigated, indicating that at the current capital cost of stationary $LiFePO_4$ batteries and the present fixed feed-in-tariff (NZ$0.08/kWh), it is not economically viable to cycle the storage for arbitrage reasons alone. In conclusion, this paper highlights the critical need to incorporate probabilistic optimisation techniques and emphasises the importance of sizing and scheduling co-optimisation when designing hybrid ESSs for integration into grid-connected micro-grids.

1. Introduction

The ever-increasing penetration of distributed energy resources (DERs) into the existing power networks presents challenges in terms of balancing electricity supply and demand, requiring novel interventions to improve the grid flexibility and resource adequacy margins [1–4]. To date, the suggested mechanisms to address the need for additional operating reserves and high ramp rates in highly renewable power systems have included additional dispatchable generation allocation, renewable energy curtailment, demand-side flexibility provisions, and energy storage procurements [5–7]. However, reserving unloaded capacity on dispatchable generators (including thermal generators and hydropower plants) and renewable energy curtailment are becoming increasingly controversial in terms of financial viability and environmental responsibility [8–10].

Also, not only are the required investments in information and communication technologies (ICT) infrastructure for automated small- to medium-scale demand response still prohibitive, but also the impact of the underlying behavioural factors in optimising demand response is still less well understood – thereby, potentially carrying a risk of failure in meeting the contract performance requirements when demand response events are declared [11–15]. In contrast, the rapidly declining cost of energy storage technologies – particularly batteries and super-capacitors (SCs) – is providing system operators with a cost-efficient resource to effectively manage variability in generation and load, as well as the volatility of wholesale electricity prices [16–18].

The applications for which an energy storage technology is useful are determined by its corresponding power and energy capacities. Put differently, the potential applications of storage technologies are typically classified by the duration of discharge needed for a particular service. Additionally, different energy storage systems are associated

* Corresponding author.
E-mail address: soheil.mohseni@ecs.vuw.ac.nz (S. Mohseni).

https://doi.org/10.1016/j.est.2023.109172
Received 6 May 2023; Received in revised form 11 September 2023; Accepted 2 October 2023
Available online 12 October 2023

Nomenclature

a_{PV} area of each PV panel [m^2]
$AH^{min}_{B/SC}$ minimum allowable autonomy hour of the battery/SC bank [h]
α, β shape parameters of the beta distribution
b constant defining the shape of the logarithmic spiral
c, k scale and shape parameters of the Weibull distribution
C^{min}_{B}, C^{min}_{SC} end-of-life capacity of the battery/SC bank [kWh]
$C_B(0)$, $C_{SC}(0)$ initial capacity of the battery/SC bank [kWh]
$C_B(cycle)$, $C_{SC}(cycle)$ remaining capacity of the battery/SC bank with respect to the cycle count [kWh]
CC capital cost [$]
CL component lifetime [years]
CRF capital recovery factor
C^{i}_{exch} cost of net power exchanges in year i [$]
$cycle^{max}_{B}$, $cycle^{max}_{SC}$ maximum cycle count of the battery/SC bank
D_{ij} distance between moth i and flame j
Δt duration of time-step [h]
η_{PV}, η_{I} efficiency of PV panels and inverters [%]
$\eta_{ch,B/SC}$ charging efficiency of the battery/SC bank [%]
$\eta_{dch,B/SC}$ discharging efficiency of the battery/SC bank [%]
E^{RSc}_{x} expected value of variable x over the reduced scenario realisations
$E_{B/SC}(t)$ energy in the battery/SC bank at time-step t [kWh]
F_j position of flame j
$\boldsymbol{FiT}$ vector of feed-in-tariff [$/kWh]
GOS^{min}_{MG} minimum allowable grid outage survivability [h]
ir real interest rate [%]
$LPSP^{max}$ maximum allowable loss of power supply probability
M_i position of moth i
$N_{PV,ins}$, $N_{WT,ins}$, $N_{I,ins}$ existing installed quantity of PV panels, wind turbines, and inverters
N_c optimal quantity/capacity of component c in the candidate pool: battery (B), super-capacitor (SC), and inverter (I)
N^{max}_{B}, N^{max}_{SC}, N^{max}_{I} maximum allowable quantity of the battery packs, SC packs, and inverters
N_{RSc} number of reduced scenarios
NPV_{exch} net present value of power exchanges [$]
NPC_B, NPC_{SC}, NPC_I net present cost of the battery bank, SC bank, and inverter [$]
N_S optimal quantity of storage modules
$O\&M$ operation and maintenance cost [$]
$P_{PV}(t)$, $P_{WT}(t)$ power output from the PV plant and wind turbines at time-step t [kW]
$P_{WT,r}$, $P_{I,r}$ rated capacity of wind turbines and inverters [kW]
$P_{ex/sh}(t)$ excess/shortage power at time-step t [kW]
$P^{L}_{ex/sh}(t)$, $P^{H}_{ex/sh}(t)$ low-frequency and high-frequency components of excess/shortage power at time-step t [kW]
$P^{max}_{ch,B/SC}$, $P^{max}_{dch,B/SC}$ charge/discharge power capacity of the battery/SC bank [kW]
$P_G(t)$ total on-site power generation at time-step t [kW]
$\boldsymbol{P_{ch,B}}$, $\boldsymbol{P_{dch,B}}$, $\boldsymbol{P_{ch,SC}}$, $\boldsymbol{P_{dch,SC}}$ vector of hourly battery charging power, battery discharging power, SC charging power, and SC discharging power [kW]
$\boldsymbol{P_{ex}}$, $\boldsymbol{P_{im}}$ vector of grid exports and imports [kW]
$\boldsymbol{P_L}$ vector of load power demand [kW]
$\boldsymbol{P_{RE}}$ vector of total renewable energy generated [kW]
PL project lifetime [years]
$\rho_{RSc}(Sc_{SI}, Sc_{WS}, Sc_{LD}, Sc_{WP})$ probability of reduced scenario vector X^{RSc}
$\rho_{Sc_{SI}}$, $\rho_{Sc_{WS}}$, $\rho_{Sc_{LD}}$, $\rho_{Sc_{WP}}$ probability of scenario Sc_{SI}, Sc_{WS}, Sc_{LD}, and Sc_{WP}
$\rho_{x,Sc}$ probability of uncertain variable x in scenario Sc
$\boldsymbol{\pi}$ vector of wholesale electricity prices [$/kWh]
Q_{life}, Q_{thr} lifetime throughput of storage [kWh] and annual storage throughput [kWh/year]
r a random number in the range $[-1, 1]$
RC replacement cost [$]
R_S storage lifetime [years]
$s(t)$ global horizontal irradiance at time-step t [kW/m^2]
S logarithmic spiral function
Sc_{SI}, Sc_{WS}, Sc_{LD}, Sc_{WP} value of solar irradiance [kW/m^2], wind speed [m/s], load demand [kWh], and wholesale price [$/kWh] in scenario Sc
SV salvage value [$]
$SPPW$ single-payment present-worth factor
SSR^{min} minimum allowable self-sufficiency ratio [%]
T number of time-steps in the operational planning horizon
$v(t)$, v_{ci}, v_{co}, v_r wind speed at time-step t, wind turbine's cut-in wind speed, cut-out wind speed, and wind turbine's rated wind speed [m/s]
$\omega_{Sc_{SI},Sc_{WS},Sc_{LD},Sc_{WP}}$ binary variable corresponding to the existence or absence of an original scenario in the set of reduced scenarios
$\bar{x}_{x,Sc}$ value of uncertain variable x in scenario Sc
X^{Sc}, X^{RSc} original scenario vector and reduced scenario vector
μ mean value
σ variance value
$\sigma_{B/SC}$ self-discharge rate of the battery/SC bank [%/day]
$\Gamma(z)$ gamma function

with different learning curves and different rates of technology advancements for improved efficiency. This brings to light the importance of producing a cost-optimal mix of different energy storage devices necessary to support cost-effective storage deployment – driven by the need for variable net demand smoothing [19–23].

In this context, hybrid energy storage systems (HESSs) integrate two or more energy storage technologies with complementary characteristics to reduce costs and energy curtailment, improve system efficiency, minimise the overall storage capacity, and prolong system lifetime by optimally operating each technology across the time scale it is specifically designed for – in accordance with the duration of energy storage capacity per unit of power capacity [24–28].

As the above discussion suggests, supporting renewable and sustainable energy systems with energy storage solutions has been found to be one of the most effective interventions to improve their overall efficiency, resulting in lighter footprints, higher robustness, and improved cost-efficiency. To this end, a key design problem is to yield the optimal storage sizing solution that offers the best compromise between the total discounted costs incurred and the technical improvements from hybridising different storage technologies.

More specifically, considering multiple energy storage technologies with different technical characteristics increases the complexity of the associated optimal storage sizing problem significantly. In large part, this is because an intelligent control strategy needs to be integrated into the storage capacity planning model to optimally determine the share of each storage medium in serving the total load demand – in compliance with the time scale relevant to the technical capabilities of each technology.

1.1. Literature review: knowledge gaps

A recent, growing body of the energy storage sizing literature has focused on designing capacity planning approaches tailored to multi-energy-storage-technology-integrated renewable and sustainable energy systems. Accordingly, a variety of methodologies and approaches have been developed to optimally size hybrid storage systems, either independently or jointly with other distributed generation and storage components, which are reviewed in detail in [6,21,22,29–33].

Table 1 presents a summary of the most notable previous studies on the optimal capacity planning of HESSs. The table, additionally, positions this paper within the identified content gaps and previously neglected factors in the optimal hybrid storage investment planning as indicated by '✘' marks.

The literature review has identified several methodological and knowledge gaps in optimal HESS asset allocation research, namely:

- *Lack of comprehensive, high-quality uncertainty-aware approaches:* Assuming perfect long-term input data forecasts – or, put differently, ignoring the uncertainty associated with input data forecasts – is common practice in the long-term HESS investment planning literature. Although their potential benefit in narrowing reality gaps has been demonstrated in several distributed energy resource optimisation areas, stochastic models applied to the HESS capacity planning problem remain underutilised.
- *Underrepresented usage of joint operational and investment optimisation methods:* While practically all the HESS models reviewed consider the life-cycle cost as a decision criterion, co-optimising the short-term energy scheduling and investment planning, is seldom reported. There are a few instances in the literature where the optimal HESS portfolio and optimal dispatch schedules are concurrently determined at hourly time fidelity. However, as far as can be ascertained, no scholarly attention has been given to formulating an optimal HESS design problem where a model predictive control-based optimal dispatch strategy over a moving 24-hour horizon is nested within.
- *Negligence of storage degradation effects and projected storage cost declines:* It is common knowledge that assuming energy storage devices do not degrade over cycle life is not a reasonable approximation of reality and there is strong evidence to support the proposition that steep declines in storage procurement costs are projected [67,68]. However, the characterisation of the cycle-induced HESS degradation and the consideration of the expected reductions in the replacement costs of storage technologies are less well explored in the literature on HESS planning – with addressing this issue implying potential positive impacts on reducing the simulation-to-reality gaps.
- *A narrow focus on state-of-the-art meta-heuristics:* Although their superiority to conventional meta-heuristics and exact mathematical optimisation algorithms has been demonstrated in many instances, fundamentally new meta-heuristic optimisation algorithm-based capacity planning models applied to HESS capacity planning remain underutilised. In particular, a moth-flame optimisation algorithm (MFOA)-based investment planning approach is found to be non-existent in the HESS sizing literature.

1.2. Novel contributions

To address the above-mentioned knowledge gaps, this paper presents a two-stage, meta-heuristic-based, robust, stochastic, long-term HESS capacity planning optimisation modelling framework tailored to hybrid battery/SC systems. Among various candidates, the low-pass energy filter, first introduced by Xu et al. [69], was adapted for application to the hybrid battery/SC sizing problem to produce the best-compromise scheduling solution in terms of energy density and power density due to its fewer model parameters compared to the peer frequency-based methods for the decomposition of the supply-demand power mismatch signal. Specifically, the proposed model features the following four key novel generalisations, each addressing one of the above-mentioned literature gaps:

- *General data-driven, large-scale, scenario-led stochastic programming:* The uncertainty associated with long-term input data forecasts, such as solar irradiance, wind speed, load demand, and wholesale power price, is quantified using probabilistic scenarios generated by discretising the corresponding hour-specific probability density functions (PDFs).
- *Coordinated, system-level design and dispatch co-optimisation over a moving one-day look-ahead period:* A model predictive control-oriented linear programming energy management optimisation model is nested within the meta-heuristic-based HESS capacity allocation approach to optimise the operational schedules of the hybrid storage over a moving 24-hour energy dispatch horizon.
- *Quantification of dynamic energy storage degradation and incorporation of learning curve costs:* A linearized dynamic degradation model is used to characterise the cycle-induced capacity losses of stationary LiFePO4 Li-ion battery packs and electric double-layer capacitor (EDLC) SC modules. In addition, this study incorporates the effects of learning curve costs, reflecting the reduction in overall costs over time as a result of increased experience in energy storage system deployment and operation.
- *MFOA-based design optimisation:* The integrated approach to optimise the hybrid storage capacity procurement cost constitutes the first HESS optimisation study of any kind that implements the state-of-the-art meta-heuristic algorithm MFOA. The MFOA [70] was chosen from a pool of >40 state-of-the-art evolutionary techniques to search for and select the optimal hybrid battery/SC design. Particularly, the MFOA was chosen because its statistical outperformance to the algorithms in the candidate pool has recently been verified in micro-grid (MG) capacity planning applications [71–73].

1.3. Paper organisation

The remainder of the paper is organised as follows. Section 2 presents a hybrid battery/SC storage-integrated test-case MG system, while additionally presenting the proposed low-pass filter-based, degradation-aware, optimal day-ahead scheduling strategy. Section 3 mathematically defines the proposed meta-heuristic-based probabilistic sizing model tailored to grid-connected hybrid battery/SC community MGs, within which the optimal scheduling strategy is nested. The case study is detailed in Section 4 before the modelling results are discussed in Section 5. Finally, Section 6 draws conclusions and suggests areas for future work.

2. Test-case hybrid battery/SC-integrated micro-grid

A DC-coupled, grid-connected residential MG, shown in Fig. 1, is considered. The existing system consists of solar photovoltaic (PV) and wind turbine (WT) generation technologies, which need to be supported by a hybrid battery/SC storage.

While the uni- and bi-directional power electronics devices connecting the system components to the common DC bus, as well as the multi-mode inverter and transformer, are modelled by constant efficiencies, the following components are modelled in more detail.

2.1. PV panels

At each time-step t, the PV generation system's output power is given by [74]:

$$P_{PV}(t) = N_{PV,ins} \cdot \eta_{PV} \cdot a_{PV} \cdot s(t), \quad (1)$$

where $N_{PV,ins}$ is the existing installed quantity of PV panels, η_{PV} is the

Table 1
Summary of the most notable previous studies on the optimal planning of HESSs.

Reference	Storage technologies	HESS operating strategy	Design optimisation approach	Uncertainty treatment	Energy scheduling optimisation	Consideration of degradation effects	Consideration of projected replacement cost reductions
[34]	Battery/FC	SMRB	Peak demand-based capacity planning	✘	✘	✘	✘
[35]	Battery/SC	Lagrange multipliers	Improved PSO, improved simulated annealing	✓	✘	✘	✘
[36]	Battery/SC	Low-pass filter	Peak demand-based capacity planning	✘	✘	✘	✘
[37]	Battery/SC	Low-pass filter	Multi-objective GA	✘	✘	✓	✘
[38]	Battery/TES	SMRB	Cuckoo optimisation algorithm	✓	✓	✘	✘
[39]	Battery/FC	Extended-power pinch analysis	Peak demand-based capacity planning	✘	✘	✘	✘
[40]	Pumped-hydro/CAES/ battery/flywheel	MMRB	Peak demand-based capacity planning	✘	✘	✘	✘
[41]	Unspecified technologies allocated to the very short-term, short-term, intra-day, and inter-day time-scales	DFT	Ad-hoc design based upon the expected peak load	✘	✘	✘	✘
[42]	Battery/FC	Lagrange multipliers	Scenario-based modelling	✘	✘	✘	✘
[43]	Battery/SC	First-order passive low-pass filter	Ragone-plot-guided optimisation	✘	✘	✘	✘
[44]	Battery/SMES	Arbitrarily weighted power mismatch stabilisation	Ad-hoc design based upon the expected peak load	✘	✘	✘	✘
[45]	Battery/FC	SMRB	Ant colony optimisation	✘	✘	✘	✘
[46]	Battery/FC	SMRB	HOMER software	✘	✘	✘	✘
[47]	Battery/SC	DFT	Ad-hoc design based upon the expected peak load	✘	✘	✘	✘
[48]	Battery/SC	Lagrange multipliers	Linear programming	✘	✓	✘	✘
[49]	Battery/FC	MMRB	PSO	✘	✓	✘	✘
[50]	Battery/FC	MMRB	GA	✓	✓	✓	✘
[51]	Battery/TES	SMRB	Mixed-integer linear programming	✘	✘	✘	✘
[52]	Battery/TES	SMRB	Ad-hoc design based upon the expected peak load	✘	✘	✘	✘
[53]	Battery/SC	DFT	GA	✘	✘	✘	✘
[54]	Battery/FC	DFT	Scenario-based modelling	✘	✘	✘	✘
[55]	Battery/SC/flywheel/CAES	Multi-attribute utility theory	Unspecified exact mathematical optimisation	✓	✘	✘	✘
[56]	Battery/SC	Low-pass filter	PSO	✘	✘	✘	✘
[57]	Lead acid battery/lithium polymer battery/flywheel/SC	Switched decay ordinary differential equation	Unspecified exact mathematical optimisation algorithm	✘	✘	✘	✘
[58]	Battery/SC	SMRB	Multi-objective GA	✘	✘	✘	✘
[26]	Battery/SC/FC	Pinch analysis	Design space approach	✘	✘	✘	✘
[59]	Battery/SC	Low-pass filter	Differential evolution	✘	✓	✘	✘
[60]	Battery/FC	SMRB	GA	✘	✘	✘	✘
[61]	Battery/TES	SMRB	Evolutionary-PSO	✘	✘	✓	✘
[62]	Battery/battery	SMRB	Mixed-integer nonlinear programming	✘	✘	✓	✘
[63]	Battery/pumped-hydro	MMRB	Grey wolf optimiser	✘	✘	✘	✓
[64]	Battery/SC	Low-pass filter	Whale optimisation algorithm	✘	✘	✓	✘
[65]	Battery/SC	SMRB	Dynamic programming	✘	✘	✓	✘
[66]	Battery/SC/SMES	MMRB	Nonlinear programming	✘	✘	✘	✘
This study	Battery/SC	First-order passive low-pass energy filter	Moth-flame optimisation algorithm	✓	✓	✓	✓

Key: CAES = Compressed Air Energy Storage, DFT = Discrete Fourier Transform, FC = Fuel Cell, GA = Genetic Algorithm, MMRB = Mix-Mode Rule-Based, PSO = Particle Swarm Optimisation, SC = Super-Capacitor, SMES = Superconducting Magnetic Energy Storage, SMRB = Single-Mode Rule-Based, TES = Thermal Energy Storage.

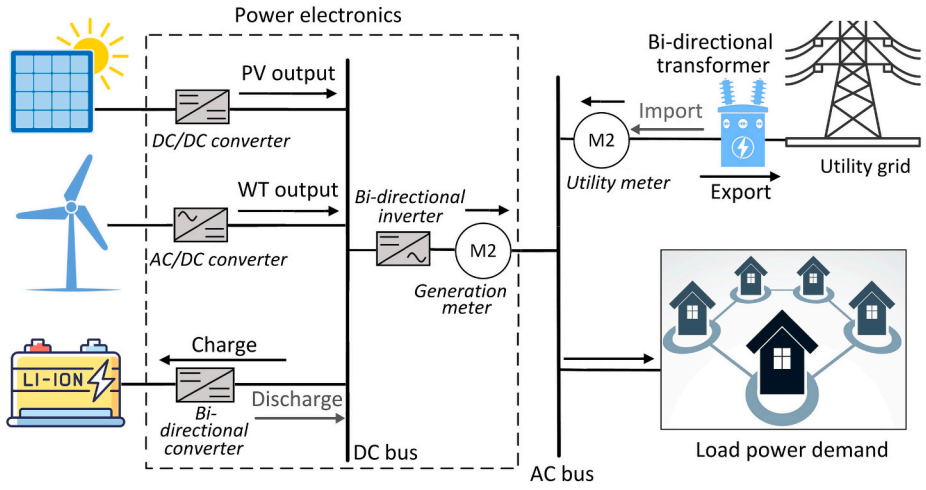

Fig. 1. Schematic of DC-coupled grid-connected solar PV/WT/battery/SC MG system.

overall efficiency of the plant (taken as a constant for simplification), a_{PV} is the area of each panel [m^2], and $s(t)$ is the global horizontal irradiance at time-step t [kW/m^2].

2.2. Wind turbines

The power output from the WT generation system can be calculated by [75]:

$$P_{WT}(t) = N_{WT,ins} \times \begin{cases} 0 \text{ if } v(t) \le v_{ci} \text{ or } v(t) \ge v_{co}, \\ \frac{P_{WT,r}}{v_r^3 - v_{ci}^3} v^3(t) - \frac{v_{ci}^3}{v_r^3 - v_{ci}^3} P_{WT,r} \text{ if } v_{ci} < v(t) \le v_r, \\ P_{WT,r} \text{ if } v_r < v(t) < v_{co}, \end{cases} \quad (2)$$

where $N_{WT,ins}$ is the existing installed quantity of WTs, $v(t)$ is wind speed at time-step t [m/s], $P_{WT,r}$ is the rated capacity of each turbine [kW], while v_r, v_{ci}, and v_{co} are the rated, cut-in, and cut-out wind speeds, respectively [m/s].

2.3. Hybrid battery/SC bank

The energy filter concept is used in this study to smooth the charging power and discharging power of the battery bank by allocating power surges to the SC bank. The energy filter is realised using a first-order passive low-pass filter, which decomposes an hourly excess/shortage power signal into high- and low-frequency components, which are respectively addressed by the SC and battery banks. Fig. 2 illustrates the concept of the energy filter for application to the decomposition of excess/shortage power signals (refer to Fig. A1 in the Appendix for the power rating versus rated energy capacity comparison for battery and super-capacitor systems across various storage systems).

The energy filter's transfer function is given by [69]:

$$f(s) = \frac{\omega_n^2}{s^2 + (\omega_n/Q)s + \omega_n^2}, \quad (3)$$

where Q denotes the first-order passive low-pass filter's quality factor and ω_n represents the associated cut-off frequency.

More specifically, Q (quality factor) indicates the damping characteristics of the system. It provides insights into how quickly or slowly the system's oscillations decay over time. Also, ω_n (natural frequency)

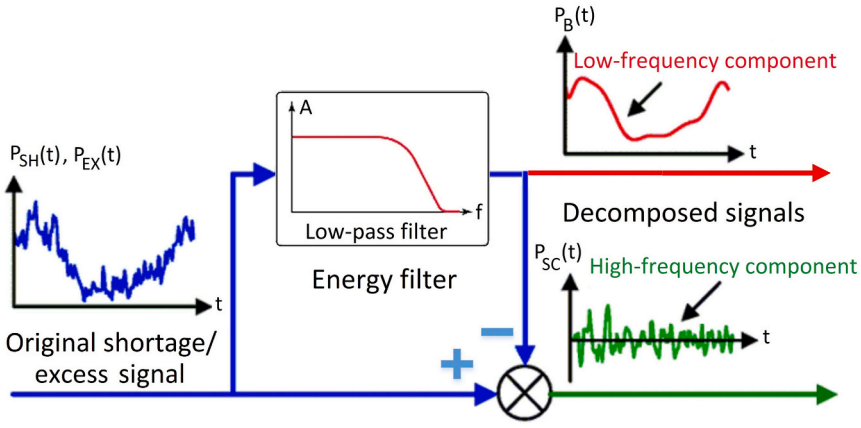

Fig. 2. Illustration of the energy filter concept's application to the battery/SC HESS. (Adapted from [69]).

represents the inherent frequency at which the hybrid energy storage system naturally oscillates or responds to external influences. It characterises the system's intrinsic dynamics. Further, s (complex frequency variable) represents the complex frequency variable, which accounts for the Laplace domain where the transfer function operates. It allows for analysing the system's dynamic response to different inputs and conditions.

By applying the filter, the low-frequency component of the shortage/excess power (addressed by the battery bank) can be obtained as:

$$\frac{P^{L}_{ex/sh}}{P_{ex/sh}} = \frac{\omega_n^2}{\left(\frac{1-z^{-1}}{\Delta t}\right)^2 + \frac{\omega_n}{Q}\frac{1-z^{-1}}{\Delta t} + \omega_n^2}, \tag{4}$$

$$P^{L}_{ex/sh}(t) = \frac{\omega_n^2 \Delta t^2 P_{ex/sh}(t) + \left(2 + \frac{\omega_n \Delta t}{Q}\right) P^{L}_{ex/sh}(t-1) - P^{L}_{ex/sh}(t-2)}{1 + \frac{\omega_n \Delta t}{Q} + \omega_n^2 \Delta t^2}, \tag{5}$$

where the value of the low-frequency component of the energy excess/shortage signal, $P^{L}_{ex/sh}$, in the first two time-steps is assumed to be equal to the corresponding value of $P_{ex/sh}$. That is, $P^{L}_{ex/sh}(1) = P_{ex/sh}(1)$ and $P^{L}_{ex/sh}(2) = P_{ex/sh}(2)$.

The high-frequency component of the excess/shortage signal, $P^{H}_{ex/sh}$, which is directed to the SC bank, can accordingly be obtained as:

$$P^{H}_{ex/sh}(t) = P_{ex/sh}(t) - P^{L}_{ex/sh}(t). \tag{6}$$

2.3.1. Cycle counting algorithm

To systematically count the heterogeneous cycles of the battery and SC banks, the three-point rainflow-counting algorithm is employed in this paper [76,77]. The algorithm can translate a spectrum of varying states of charge into a set of discrete full- and half-change cycles as a function of cycle amplitude. To this end, first, the associated state-of-charge (SOC) profile is converted into a series of minima and maxima (known as reversals), where the delta SOC changes sign. The cycles are counted by using a moving reference point of the series, Z, as well as a moving ordered three-point subset with the following features [78]:

- The first and second points are collectively denoted by Y.
- The second and third points are collectively denoted by X.
- The sets of ordered pairs X and Y are sorted chronologically but are not necessarily consecutive points in the SOC profile.
- The range of X, denoted by $r(X)$, is defined as the absolute difference between the amplitudes of the first and second points. The definition of $r(Y)$ is analogous.

In this context, Fig. 3 illustrates the process flow of the three-point rainflow-counting algorithm [78].

Fig. 4, additionally, illustrates the application of the rainflow-cycle-counting algorithm on a typical representative SOC profile [25]. In the figure, the full cycles are represented by the planes enclosed by the mustard yellow triangles, whereas the half-cycles are represented by the planes enclosed by the triangles diagonally shaded in light blue. As the figure shows, the representative SOC profile contains three full cycles – the triangular regions B-A′-B′, J-K′-J′, and I-F-I′ – and four half-cycles – the triangular regions C-D-C′, G-H-G′, L-M-L′, and N-O-N′.

In this paper, the MATLAB's built-in 'rainflow' function [78] is used to estimate the battery and SC cycle counts as part of calculating the application-specific expected cycle life of the battery and SC banks, which are then adjusted for the cycle-induced degradation and the effects of depth of discharge (DOD) on the cycle life according to the procedures described in the next sub-section.

2.3.2. Battery/SC degradation and DOD effects

The cycle-induced degradation of the $LiFePO_4$ Li-ion battery bank is modelled by the linear function in Eq. (7) [50]. The employed capacity fade characterisation technique is illustrated in Fig. 5.

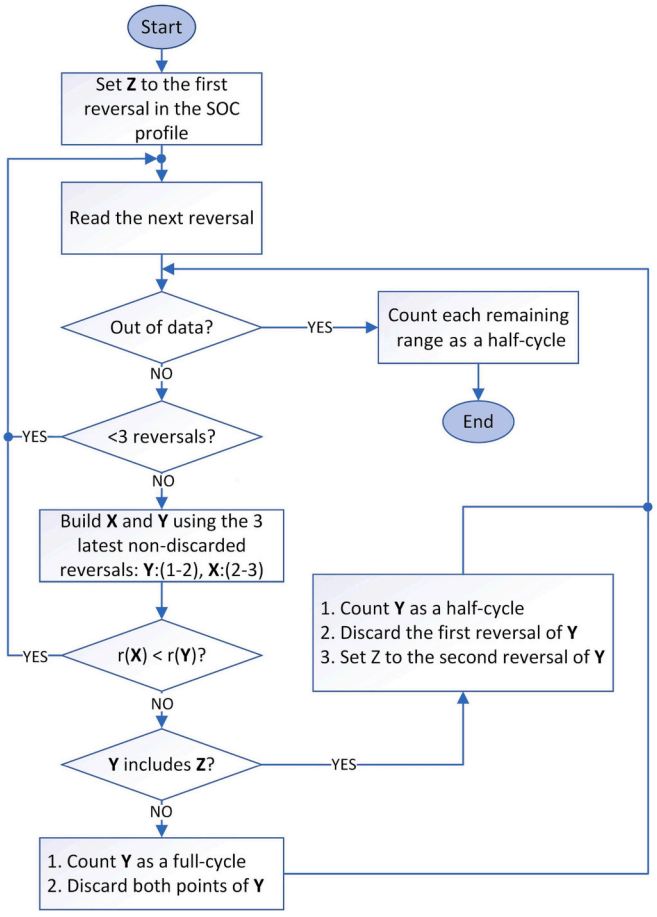

Fig. 3. Illustration of the three-point rainflow-counting algorithm. (Adapted from [78]).

$$C_B(cycle) = C_B(0) - \frac{C_B(0) - C_B^{min}}{cycle_B^{max}} cycle, \tag{7}$$

where $C_B(0)$ denotes the initial capacity of the battery, C_B^{min} is the expected battery capacity at its end-of-life phase, and $cycle_B^{max}$ denotes the manufacturer-provided maximum battery cycle count. A similar process characterises the degradation of the SC bank.

Moreover, to account for the impact of the DOD on the expected average cycles, first, the best-fit curve for the manufacturer-provided cycles-to-failure with respect to the DOD data is produced. The following logarithmic polynomial function describes the relationship between the battery's cycles-to-failure and DOD characteristics [79]:

$$CTF = a_0 + a_1 DOD^{-1} + a_2 DOD^{-2} + a_3 DOD^{-3}, \tag{8}$$

where CTF denotes the cycles-to-failure, DOD is the depth-of-discharge, with a_0, a_1, a_2, and a_3 denoting the curve fitting coefficients.

Then, the DOD-adjusted cycle-life expectancy of the battery system can be obtained from the following equation [79]:

$$L_{B,C} = \sum_{t=1}^{T} \frac{CTF(DOD_B(100))}{CTF(DOD_B(t))}, \tag{9}$$

where $CTF(DOD_B(100))$ is the battery's specified cycle life at 100 % DOD and $CTF(DOD_B(t))$ is the battery's cycles-to-failure determined for the t-th hour of the MG operation, while adjusting for the DOD. Note that 1 full cycle means 100 % of battery energy charged and discharged.

On the other hand, assuming that battery enclosures with full air

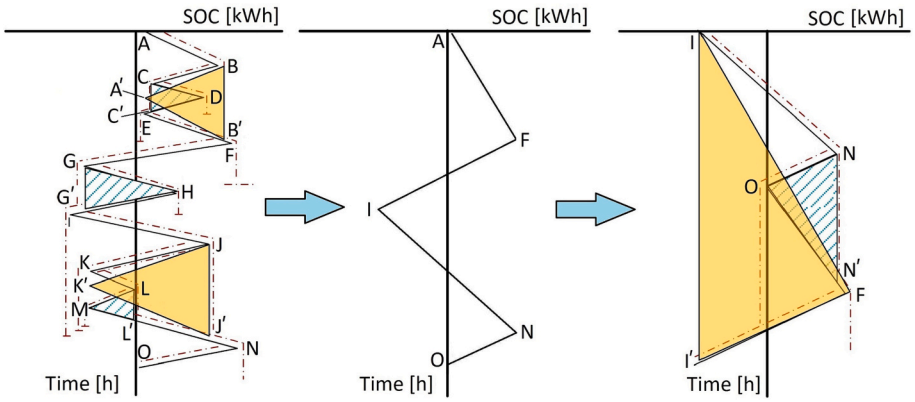

Fig. 4. Illustrative application of the three-point rainflow-counting algorithm to a typical representative SOC profile. (Adapted from [25]).

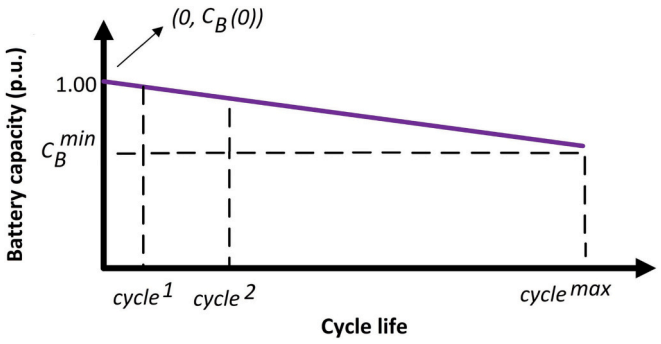

Fig. 5. Characterisation of the battery bank degradation effect. (Adapted from [50]).

conditioning and temperature control are in place, a linear calendar-life aging estimation model as a function of the SOC can be used, as follows [79]:

$$CD_{1h}(t) = b_0 + b_1 SOC(t), \tag{10}$$

where $CD_{1h}(t)$ and $SOC(t)$ respectively denote the hourly calendar-induced capacity loss and SOC, while b_0 and b_1 are the coefficients obtained from fitting a linear curve to the associated manufacturer-provided empirical data collected from accelerated life tests.

Accordingly, the cumulative calendar-driven battery capacity loss at the i-th hour of the MG operation over its lifetime can be calculated as [79]:

$$CD(i) = \sum_{i=1}^{I} CD_{1h}(i), \tag{11}$$

where $I_i = \{i_1, i_2, \ldots, I\}$ is the total set of useful battery operating times, ranging from baseline time i_0 (the first hour of system operation) to final time I (the elapsed time before a battery becomes unusable). For example, assuming an expected battery life of 15 years and hourly data granularity, $I = 8760 \times 15 = 131{,}400$.

In this light, by taking a superposition approach to calculating the battery end-of-life, Eq. (11) can be modified to factor calendar-induced battery degradation into the analysis, as follows:

$$C_B(cycle, i) = C_B(0) - \left(\frac{C_B(0) - C_B^{min}}{cycle_B^{max}} cycle + CD(i) \right). \tag{12}$$

3. Probabilistic optimal capacity planning of hybrid battery/SC systems

The proposed two-stage method for the coordinated, system-level design and dispatch co-optimisation of hybrid battery/SC systems integrated into grid-connected MGs consists of an outer optimal sizing stage and a nested dispatch optimisation loop, as explained in the following sub-sections.

3.1. Optimal operational scheduling stage

This sub-section details the hourly-basis rule-based operational planning strategy developed to optimally schedule the charging/discharging of the hybrid storage system with reference to the day-ahead, local generation, load demand, and wholesale electricity prices. The operational strategy is designed based on linear programming formulations to optimally control the operation of the hybrid storage system assuming that the 24 h' worth of wholesale prices, local generation, and demand for the next day are available. Notably, the storage follows the general arbitrage strategy of 'charge cheaply, discharge discreetly'.

The day-ahead energy management optimisation problem to maximise the day-ahead profit is defined in Eqs. (13)–(22). Bold-face characters refer to 24-hour column vectors. It should be noted that the operational strategy is inspired by the linear programming formulations proposed by Pimm et al. [80].

$$max\ Pr = \boldsymbol{P_{ex}} \boldsymbol{Fi} \boldsymbol{T}^T \Delta t - \boldsymbol{P_{im}} \boldsymbol{\pi}^T \Delta t - 10^{-6} \|\boldsymbol{u}\|_1, \tag{13}$$

subject to:

$$\boldsymbol{P_{im}} - \boldsymbol{P_{ex}} = \boldsymbol{P_L} - \boldsymbol{P_{RE}} + \boldsymbol{P_{ch,B}} - \boldsymbol{P_{dch,B}} + \boldsymbol{P_{ch,SC}} - \boldsymbol{P_{dch,SC}}, \tag{14}$$

$$E_{B/SC}(t) = E_{B/SC}(t-1) \cdot \left(1 - \sigma_{B/SC} \cdot \Delta t\right) + \eta_{ch,B/SC} \cdot P_{ch,B/SC}(t) \cdot \Delta t - \frac{P_{dch,B/SC}(t) . \Delta t}{\eta_{dch,B/SC}} \ \forall t, \tag{15}$$

$$C_{B/SC}^{min} \le E_{B/SC}(t) \le C_{B/SC}(cycle)\ \forall t, \tag{16}$$

$$0 \le P_{ch,B/SC}(t) \le u_{ch}(t) \cdot P_{ch,B/SC}^{max}\ \forall t, \tag{17}$$

$$0 \le P_{dch,B/SC}(t) \le u_{dch}(t) \cdot P_{dch,B/SC}^{max}\ \forall t, \tag{18}$$

$$u_{ch}(t) + u_{dch}(t) = 0\ \forall t, \tag{19}$$

$$0 \le P_{im}(t) \le u_{im}(t) \cdot \left(N_I \cdot P_{I,r} + P_{I,ins}\right)\ \forall t, \tag{20}$$

$$0 \le P_{ex}(t) \le u_{ex}(t) \cdot \left(N_I \cdot P_{I,r} + P_{I,ins}\right)\ \forall t, \tag{21}$$

$$u_{im}(t) + u_{ex}(t) \leq 1 \forall t, \tag{22}$$

where Pr denotes the 24-hour vector of day-ahead profits, P_{im} represents the imported power, P_{ex} is the exported power, P_L is the load power, P_{RE} is the renewable energy generation, FiT denotes the feed-in tariff, π is the wholesale electricity price, $P_{ch,B}$ and $P_{dch,B}$ respectively denote the charging and discharging power of the battery bank, $P_{ch,SC}$ and $P_{dch,SC}$ respectively represent the charging and discharging power of the SC bank, $E_{B/SC}$ is the energy content of the battery/SC bank, $\sigma_{B/SC}$ is the self-discharge rate of the battery/SC bank, $\eta_{ch,B/SC}$ and $\eta_{dch,B/SC}$ respectively denote the charging and discharging efficiencies of the battery/SC bank, $P_{ch,B/SC}$ and $P_{dch,B/SC}$ respectively denote the charging power and discharging power of the battery/SC bank, $P^{max}_{ch,B/SC}$ and $P^{max}_{dch,B/SC}$ respectively represent the maximum charging and discharging power of the battery/SC bank, u_{ch} and u_{dch} are binary variables used to ensure that charging and discharging do not occur concurrently, u_{im} and u_{ex} guarantee the non-simultaneous importing and exporting, N_I is the optimal size of the inverter to be installed, $P_{I,r}$ is the rated power of the inverter to be installed, while $P_{I,ins}$ denotes the capacity of the existing installed inverter.

Particularly, Eq. (14) defines the power balance constraint, ensuring that the imported and exported power, along with the load power, onsite renewable power generation, as well as the charging and discharging power components of the energy storage devices – which define the energy content of the battery bank at each time-step in Eq. (15) – are in equilibrium.

The final component of the objective function in Eq. (13), namely $10^{-6}\|\boldsymbol{u}\|_1$, penalises the solutions that entail unprofitable cycling by accommodating the net present cost (NPC) of storage deterioration (due to cycling) in the day-ahead operational scheduling optimisation. It is based on the L-1 norm of the storage schedules, which can be obtained from $\|\boldsymbol{u}\|_1 = \sum_{t=t_1}^{t_1+24}\left(P_{ch,B}(t) + P_{dch,B}(t) + P_{ch,SC}(t) + P_{dch,SC}(t)\right)$.

Also, note that the lower limit on the stored energy in the battery bank in Eq. (16) is set to $(1 - DOD_B) \times C_B(cycle)$, where DOD_B is the battery's corresponding DOD. Also, the lower limit on the energy content of the SC bank is set to 0 because the EDLC SCs are considered in this study, which can be continually discharged to 100 % DOD without any long-term effects [81,82]. Also, using two binary control variables, the constraint in Eq. (19) ensures that the storage is not in both the charging and discharging modes at a single time-step. Furthermore, the exchange of power with the grid is limited by the maximum capacity of the bi-directional inverter including the existing and newly installed capacities (Eqs. (20) and (21)). Additionally, the constraint in Eq. (22) ensures that the import and export of energy are mutually exclusive events.

3.2. Optimal capacity planning stage

To determine the economic value of the investment in the hybrid battery/SC system, the concepts of net present cost (NPC) and net present value (NPV) are used in deriving the objective function.

The NPC associated with each newly installed component – battery, SC, inverter – can be obtained as [83,84]:

$$NPC = N_c \times \left(CC + RC \times SPPW + \frac{O\&M}{CRF(ir, PL)} - SV\right), \tag{23}$$

$$SPPW = \sum_{i=1}^{N} \frac{1}{(1+ir)^{CL \times i}}, \tag{24}$$

$$N = \begin{cases} \lfloor \frac{PL}{CL} \rfloor - 1 \ if \ PL \ mod \ CL = 0, \\ \lfloor \frac{PL}{CL} \rfloor \ if otherwise, \end{cases} \tag{25}$$

$$CRF(ir, PL) = \frac{ir(1+ir)^{PL}}{(1+ir)^{PL} - 1}, \tag{26}$$

$$SV = RC \times \frac{CL - \left(PL - CL \times \lfloor \frac{PL}{CL} \rfloor\right)}{CL}, \tag{27}$$

where N_c is the optimal capacity of component c, the notations CC, RC, and $O\&M$ denote the capital, replacement, and operation and maintenance costs, $SPPW$ is the single-payment present-worth factor, CRF is the capital recovery factor, ir is the interest rate, PL is the project lifetime, CL is the component lifetime, and SV is the salvage value.

The following equation can also be used to convert the cycle life of the storage components to calendar life [85]:

$$R_S = \frac{N_S \times Q_{life}}{Q_{thr}}, \tag{28}$$

where N_S is the optimal capacity of the storage component, while Q_{life} and Q_{thr} respectively denote the lifetime throughput of storage [kWh] and annual storage throughput [kWh/year] of the storage component.

Also, the NPV of the total power exchanged with the grid over the life cycle of the project can be obtained from Eq. (29).

$$NPV_{exch} = \sum_{i=1}^{PL} \frac{C^i_{exch}}{(1+ir)^i}, \tag{29}$$

where C_{exch} is the total cost of annual net energy purchased from the grid, which can be obtained as follows:

$$C_{exch} = \sum_{t=1}^{T} P_{im}(t) \cdot \pi(t) - P_{ex}(t) \cdot FiT. \tag{30}$$

Accordingly, the objective function of the optimal hybrid storage sizing problem can be defined as:

$$min \ TNPC = NPC_B + NPC_{SC} + NPC_I + NPV_{exch} + c, \tag{31}$$

where NPC_B, NPC_{SC}, and NPC_I respectively denote the net present cost of the battery bank, SC bank, and the inverter, NPV_{exch} is the net present value of power exchanges with the wider utility grid, and c is a penalty factor that adds a large positive constant to the returned value of the objective function if any of the imposed constraints are violated.

3.2.1. Constraints

The system-wide power balance constraint in Eq. (14), the energy in-store balance constraint in Eq. (15), the imposed bounds on the energy content and charging/discharging power of the battery and SC banks in Eqs. (16)–(18), the constraint that the storage cannot be both charged or discharged at a time (Eq. (19)), the imposed bounds on energy exchanges with the wider grid in Eqs. (20) and (21), and the constraint that the MG cannot be simultaneously in the charging and discharging modes in Eq. (22), need to be satisfied in the nested optimal dispatch optimisation stage. In addition, the objective function of the optimal investment planning problem (Eq. (23)) is subject to a set of constraints presented in the following sub-sections. Note that the optimal capacity planning problem is only feasible if the nested optimal operational scheduling problem is feasible.

3.2.1.1. Initial energy in-store limits. To ensure an economic serving of the peaks occurring early in the 8760-hour scheduling period, the battery and SC banks are set to be full in the first iteration, as:

$$E_{B,SC}(0) = N_{B/SC} \cdot C_{B/SC}(0). \tag{32}$$

3.2.1.2. Terminal energy in-store limits. For balanced analysis, the battery and SC banks' energy contents at the end of the operational analysis period are constrained to be equal to or exceed their initial energy contents, as:

$$E_{B/SC}(T) \geq E_{B/SC}(0). \tag{33}$$

3.2.1.3. Minimum self-sufficiency ratio. Defining the self-sufficiency ratio (SSR) as the percentage of load met using onsite DERs over the year-long energy scheduling period, the optimal sizing problem is subject to a minimum SSR, as [86]:

$$SSR \geq SSR^{min}, \tag{34}$$

$$SSR = \frac{\sum_{t=1}^{T} P_L(t) - P_{im}(t)}{\sum_{t=1}^{T} P_L(t)}, \tag{35}$$

where SSR^{min} denotes the pre-defined minimum SSR imposed, P_L is the local load, and P_{im} is the imported power.

3.2.1.4. Energy resilience constraints. The capacity planning optimisation is enforced to meet two energy resilience constraints, namely the minimum autonomy hour of the hybrid battery/SC bank and the minimum grid outage survivability, which are respectively defined as the ratio of the storage size to the mean total annual load demand and the ratio of the storage size to the mean total annual net load demand (load minus local generation), as follows [87]:

$$AH_{B/SC} \geq AH_{B/SC}^{min}, \tag{36}$$

$$AH_{B/SC} = \frac{\left(N_B \cdot P_{B,r} + N_{SC} \cdot P_{SC,r}\right)}{\left(\sum_{t=1}^{T} P_L(t)\right)/T}, \tag{37}$$

$$GOS_{MG} \geq GOS_{MG}^{min}, \tag{38}$$

$$GOS_{MG} = \frac{\left(N_B \cdot P_{B,r} + N_{SC} \cdot P_{SC,r}\right)}{\left(\sum_{t=1}^{T} P_L(t) - P_{RE,ins}(t)\right)/T}, \tag{39}$$

where $AH_{B/SC}^{min}$ is the minimum autonomy hour of the battery/SC bank imposed, N_B and N_{SC} respectively denote the optimal capacity of the battery and SC banks, $P_{B,r}$ and $P_{SC,r}$ respectively denote the rated power of the battery and SC banks, GOS_{MG}^{min} is the minimum grid outage survivability imposed, $P_{RE,ins}$ is the existing installed capacity of the renewable energy generation components, with T representing the last time-step of the operational analysis period.

3.2.1.5. Maximum loss of power supply. The optimal solution to the outer design optimisation problem needs to meet a maximum loss of power supply probability (LPSP) reliability constraint, defined as a ratio of total energy deficit to the total load demand over the year-long energy balance analysis timeframe, as [88]:

$$LPSP \leq LPSP^{max}, \tag{40}$$

$$LPSP = \frac{\sum_{t=1}^{T}(LPS(t) \times \Delta t)}{\sum_{t=1}^{T}(P_L(t) \times \Delta t)}, \tag{41}$$

$$LPS(t) = \begin{cases} P_L(t) - P_G(t) \; if \; P_L(t) > P_G(t), \\ 0 \; if \; otherwise, \end{cases} \tag{42}$$

$$P_G(t) = P_{PV}(t) + P_{WT}(t) + P_{dch,B}(t) + P_{dch,SC}(t) + P_{im}(t) \; \forall t, \tag{43}$$

where $LPSP^{max}$ is the maximum loss of power supply probability imposed, LPS denotes the amount of loss of power supply, with P_G representing an auxiliary variable that quantifies the total available power for supplying local loads from onsite generation, discharging storage components, and grid imports.

3.2.1.6. Decision variable limits. The non-negative decision variables are also upper bounded to limit the search space for computational complexity reasons, as:

$$0 \leq N_{B/SC} \leq N_{B/SC}^{max}, \tag{44}$$

$$0 \leq N_I \leq N_I^{max}, \tag{45}$$

$$0 \leq N_T \leq N_T^{max}, \tag{46}$$

where $N_{B/SC}^{max}$, N_I^{max}, and N_T^{max} respectively denote the maximum capacity of the battery/SC bank, inverter, and the transformer at the point of common coupling.

3.2.2. Optimisation algorithm

The objective function is optimised using a state-of-the-art meta-heuristic optimiser, namely the moth-flame optimisation algorithm (MFOA) [70]. The MFOA simulates the swarm behaviour of moths with respect to flames to optimise a solution to a problem. Specifically, the position of moths in the design space is updated using Eqs. (47)–(49). The updating process continues with 100 search agents until the maximum number of iterations (i.e., 200) is reached.

$$M_i = S(M_i, F_j), \tag{47}$$

$$S(M_i, F_j) = D_{ij} e^{bt} cos(2\pi r) + F_j, \tag{48}$$

$$D_{ij} = |F_j - M_i|, \tag{49}$$

where $S(M_i, F_j)$ denotes the spiral function of moth i and flame j, D_{ij} is the Euclidean distance between moth i and flame j, b is a constant that defines the shape of the logarithmic spiral, and r is a random number in the range $[-1, 1]$.

Note that in the deterministic variant of the model, the uncertain input variables – solar irradiance, wind speed, wholesale price, and load demand – are set to their expected values.

3.3. Uncertainty characterisation

The stochastic variant of the model is formulated by discretising the corresponding hour-specific continuous PDFs of the above-mentioned uncertain variables. The associated PDFs are built based on 10 years' (2012 to 2021) worth of hourly historical data for the climatic and wholesale price inputs and 10 one-year synthetic time-series derived for electricity consumption – given the lack of reliable historical load demand data for the case study area with hourly granularity. More specifically, to populate the model for generating hourly PDFs of load demand, the synthesised load demand profile for aggregated dwellings was regenerated nine times using the second-order Markov chain model developed in [89], while employing a time-dependent dummy variable to account for weekday versus weekend.

A set of multi-dimensional scenario vectors, $X^{Sc} = [Sc_{SI}, Sc_{WS}, Sc_{LD}, Sc_{WP}]$ were then generated by all possible combinations of the uncertain variables containing multiple (hourly) input values. The input values for each variable represent the mean values of the intervals obtained from discretising the corresponding PDFs, which are assigned a specific probability of occurrence. The probabilities of the scenario vectors are then calculated based on the multiplication rule of probability. Fig. 6 illustrates the PDF discretisation process for a typical representative normal distribution divided into seven equal regions. The probability of occurrence and the corresponding input value of uncertain variable x in each scenario Sc can be obtained from Eqs. (50) and (51), respectively [90].

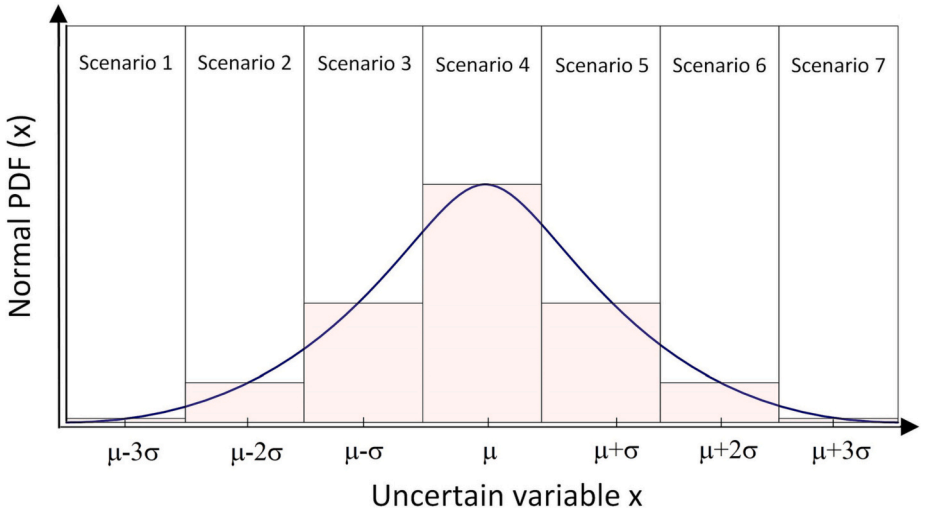

Fig. 6. Schematic illustration of scenario generation by dividing a normal PDF into equally sized intervals.

$$\rho_{x,Sc} = \int_{x_{start,Sc}}^{x_{end,Sc}} PDF(x)dx, for\ Sc = 1, 2, \ldots, N_x, \tag{50}$$

$$\bar{x}_{x,Sc} = \frac{1}{\rho_{x,Sc}} \int_{x_{start,Sc}}^{x_{end,Sc}} x.PDF(x)dx, for\ Sc = 1, 2, \ldots, N_x, \tag{51}$$

where N_x represents the total number of scenarios generated for uncertain variable x through PDF discretisation.

The two-parameter Weibull distribution is used to model hourly wind speed data, the beta distribution is used to model solar irradiance data, while the normal (Gaussian) distribution is used to model load demand and wholesale price data, as they are shown to be the best fitting distributions, respectively [91,92]. Also note that for load demand and wholesale price data, a dummy variable is used to distinguish weekday and weekend data points.

3.3.1. Beta distribution

The beta distribution for solar irradiance $0 \leq s \leq 1$ is given by [93]:

$$f(s; \alpha, \beta) = \frac{\Gamma(\alpha+\beta)}{\Gamma(\alpha)\Gamma(\beta)} s^{\alpha-1}(1-s)^{\beta-1}, \tag{52}$$

$$\alpha = \frac{\mu \cdot \beta}{1-\mu}, \tag{53}$$

$$\beta = (1-\mu)\left(\frac{\mu(1+\mu)}{\sigma^2} - 1\right), \tag{54}$$

where α and β define shape parameters of the beta distribution, while μ and σ respectively denote the mean and variance of the associated solar irradiance data records.

3.3.2. Weibull distribution

The two-parameter Weibull distribution for wind speed $v \geq 0$ is given by [93]:

$$f(v; c, k) = \frac{k}{c}\left(\frac{v}{c}\right)^{k-1} e^{-\left(\frac{v}{c}\right)^k}, \tag{55}$$

$$k = \left(\frac{\sigma}{\mu}\right)^{-1.086}, \tag{56}$$

$$c = \frac{\mu}{\Gamma\left(1+\frac{1}{k}\right)}, \tag{57}$$

where c and k denote the scale and shape parameters of the Weibull distribution, while μ and σ respectively denote the mean and variance of the associated wind speed data records.

3.3.3. Normal distribution

As mentioned above, the variability in load demand and wholesale prices are modelled by the normal distribution. The normal distribution for a Gaussian variable x can be determined as [93]:

$$f(x) = \frac{1}{\sqrt{2\pi}\sigma} e^{-\frac{1}{2}\left(\frac{x-\mu}{\sigma}\right)^2}, \tag{58}$$

where x is the corresponding random variable – load demand or wholesale prices – with μ and σ respectively denoting the mean and variance of the corresponding random data records.

3.3.4. Scenario reduction

The meta-heuristic-based stochastic storage sizing framework, which additionally entails the optimal scheduling of the hybrid storage system at a daily increment (in intervals of 1 h) for energy arbitrage,[1] is highly computationally intensive. That is, it is not computationally tractable to simulate the system for the entire set of multi-dimensional scenarios generated through PDF discretisation when dealing with multiple uncertain inputs. To put this into perspective, dividing the hour-specific PDFs generated for the four uncertain variables concerned into seven equally sized intervals results in $7^4 = 2401$ independent scenarios.

To reduce the computational complexity of the problem, while retaining the optimality of the stochastic modelling results within an acceptable limit, a mixed-integer linear programming (MILP)-based heuristic algorithm, first introduced by Karuppiah et al. [94], is adopted. The heuristic scenario reduction algorithm yields a minimum subset of a given set of multi-dimensional scenarios, which ensures that the overall probability of occurrence of a particular realisation (value) of each uncertain variable in the reduced subset equals the probability of the uncertain variable taking on that particular value. Assuming that the range of possible values for the uncertain variables has been divided into seven regions, the algorithm can be expressed mathematically as [94]:

$$minN_{RSc} = \sum_{Sc_{SI}=1}^{7} \sum_{Sc_{WS}=1}^{7} \sum_{Sc_{LD}=1}^{7} \sum_{Sc_{WP}=1}^{7} \omega_{Sc_{SI},Sc_{WS},Sc_{LD},Sc_{WP}}, \tag{59}$$

[1] It should be noted that the energy balance problem is solved for the baseline year, and then results are assumed to repeat for each of the ensuing years in the life cycle of the project.

subject to:

$$\sum_{Sc_{WS}=1}^{7}\sum_{Sc_{LD}=1}^{7}\sum_{Sc_{WP}=1}^{7}\rho_{RSc}(\,Sc_{WS},Sc_{LD},Sc_{WP})=\rho_{Sc_{SI}},\ for\ Sc_{SI}=1,2,\ldots,7, \tag{60}$$

$$\sum_{Sc_{SI}=1}^{7}\sum_{Sc_{LD}=1}^{7}\sum_{Sc_{WP}=1}^{7}\rho_{RSc}(Sc_{SI},Sc_{LD},Sc_{WP})=\rho_{Sc_{WS}},\ for\ Sc_{WS}=1,2,\ldots,7, \tag{61}$$

$$\sum_{Sc_{SI}=1}^{7}\sum_{Sc_{WS}=1}^{7}\sum_{Sc_{WP}=1}^{7}\rho_{RSc}(Sc_{SI},Sc_{WS},Sc_{WP})=\rho_{Sc_{LD}},\ for\ Sc_{LD}=1,2,\ldots,7, \tag{62}$$

$$\sum_{Sc_{SI}=1}^{7}\sum_{Sc_{WS}=1}^{7}\sum_{Sc_{LD}=1}^{7}\rho_{RSc}(Sc_{SI},Sc_{WS},Sc_{LD})=\rho_{Sc_{WP}},\ for\ Sc_{WP}=1,2,\ldots,7, \tag{63}$$

$$\sum_{Sc_{SI}=1}^{7}\sum_{Sc_{WS}=1}^{7}\sum_{Sc_{LD}=1}^{7}\sum_{Sc_{WP}=1}^{7}\rho_{RSc}(Sc_{SI},Sc_{WS},Sc_{LD}Sc_{WP})=1,\ \forall Sc_{SI},Sc_{WS},Sc_{LD},Sc_{WP}, \tag{64}$$

$$\rho_{RSc}(Sc_{SI},Sc_{WS},Sc_{LD},Sc_{WP})\le\omega_{Sc_{SI},Sc_{WS},Sc_{LD},Sc_{WP}},\ \forall Sc_{SI},Sc_{WS},Sc_{LD},Sc_{WP}, \tag{65}$$

$$0\le\rho_{RSc}(Sc_{SI},Sc_{WS},Sc_{LD},Sc_{WP})\le 1,\ \forall Sc_{SI},Sc_{WS},Sc_{LD},Sc_{WP}, \tag{66}$$

where N_{RSc} is the optimal number of reduced scenarios, $\omega_{Sc_{SI},Sc_{WS},Sc_{LD},Sc_{WP}}\in\{0,1\}$ is a binary variable that corresponds to the presence or absence of a multi-dimensional scenario X^{Sc} in the new set of scenarios, and $\rho_{RSc}(Sc_{SI},Sc_{WS},Sc_{LD},Sc_{WP})$ is the new probability assigned to the reduced scenario X^{RSc}.

Finally, the expected values of the hourly scenario outputs (value-probability pairs) for each variable x are returned as stochastic results, as follows:

$$E_x^{RSc}(t)=\sum_{rs\in RSc}\rho^{rs}(t)X^{rs}(t). \tag{67}$$

3.4. Overview of the proposed two-stage hybrid battery/SC designing model

Figs. 7 and 8 illustrate the two-stage meta-heuristic-based, stochastic solution algorithm developed for the hybrid storage capacity optimisation model. As can be seen from Fig. 7, the overall problem is separated into an outer loop storage sizing problem with a nested optimal energy scheduling problem. The optimal sizing problem (outer loop) sends a vector of decision variables (*here-and-now* design variables) to the optimal scheduling problem (inner loop).

The decision variables are treated as parameters by the optimal scheduling problem, a solution to which yields the *wait-and-see* decisions. The optimal scheduling problem is solved for every 24-hour period in the baseline year, the solutions of which are supplied to the optimal design problem to evaluate each design's fitness (total NPC). The operational planning model is formulated as a linear programming problem and solved using the MATLAB inbuilt linear programming optimiser called '*linprog*', while the long-term investment planning problem is solved using the MFOA.

Each search agent of the MFOA is represented by a vector of investment decision variables to be made over the analysis period. At each iteration of the MFOA, an investment portfolio is generated subject to the operational constraints as an output that includes the optimal DER assets' sizes and economic dispatch schedules. Then, the optimised variables are fed into the SSR, grid outage survivability, the hybrid battery/SC bank autonomy hour, and LPSP evaluation blocks to calculate the corresponding indices. The search and selection process of the MFOA is subject to a set of planning-level constraints defined based on the above-mentioned indices, which continues until the maximum number of iterations is reached.

Finally, the process is repeated for each of the clustered hourly-basis, year-long scenarios, and normal density curves that best approximate the corresponding histograms of the optimised decision variables, while the best-case, most likely case and worst-case solutions are calculated based on the 5th percentile values, expected values, and 95th percentile values, respectively.

4. Case study: Totarabank Subdivision, Aotearoa New Zealand

Located in central Wairarapa, Aotearoa New Zealand (GPS co-ordinates: 41°1′4″ S, 175°40′0″ E), Totarabank is a residential subdivision built on sustainability design criteria. It consists of eight freestanding houses, and a common building, with a total population of 14 people as of 2020 [95]. The geographical location and description of the study area are shown in Fig. 9.

To populate the model for the case of Totarabank, specific brands of equipment were chosen based on the authors' judgement of suitability for the services of interest from the options available in the Aotearoa New Zealand and Australian renewable energy asset markets.[2] Note that given the objective of the paper, only the costs associated with energy storage devices and any additional bi-directional inverter capacity required are included in the total system cost function (Eq. (31)).[3]

The economic specifications of the candidate components to be integrated into the existing grid-connected MG system are listed in Table 2, while technical assumptions, including the existing installed capacities of generation and conversion components, are summarised in Table 3. In Table 2, the replacement costs are based on projection. Also note that costs are always cited in New Zealand currency and figures depict local New Zealand time for the relevant month. Moreover, the analysis period and the real discount rate were assumed to be 25 years and 3.7 % [96], respectively.

Fig. 10 displays the monthly mean daily profiles for the expected values of meteorological, wholesale electricity price, and load demand data. The meteorological and wholesale price data consists of the rolling averages for a particular hour of the day in each month over the 10-year period 2012 to 2021, recorded at hourly intervals [108,109].[4] For the load demand data, this is the rolling average of the total forecasted consumption for a particular hour of the day over the one-year database built with hourly intervals. The electricity usage during one-hour intervals over the representative year was forecasted based on the New Zealand GREEN Grid residential electricity demand study's findings [110] in accordance with the site's population and the average number of people per household.

5. Simulation results and discussion

This section presents and discusses the results obtained from the application of the proposed model to the case study of Totarabank Subdivision. The computer code was developed in MATLAB (version R2022a). The software was run on a standard desktop computer with an Intel Core i7 3.20 GHz processor and 16 GB RAM.

[2] The following product models were chosen for non-dispatchable renewables: Trina Solar's TSM-285 solar panels [104] and Primus Wind Power's AIR 40 wind turbines [107].

[3] This study expands on the prior feasibility study carried out on the site's renewable energy potential. Accordingly, it was decided to make a simplification of fixed PV and WT sizes, which were set to the optimal values found in [115]. Although the obtained optimal renewable capacities are not yet completely implemented, they are referred to in this paper as 'existing installed' capacities to facilitate comprehension.

[4] For the wholesale price data, a time-dependent dummy variable is used to account for weekday versus weekend. It takes a value of 1 if the data point represents a weekday, and 0 if otherwise.

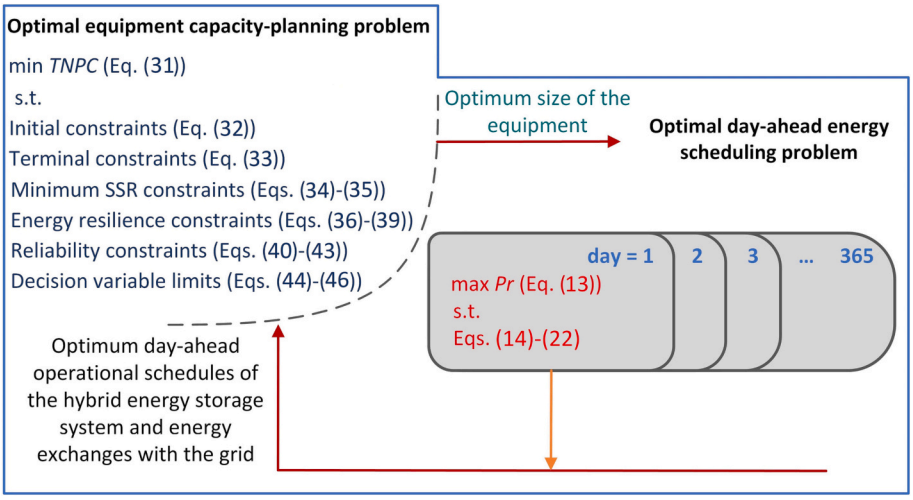

Fig. 7. Optimal stochastic storage capacity planning problem structure with nested optimal scheduling problem.

To better evaluate the effect size of each of the model's elements, simulations were conducted in four separate cases in a hierarchical manner. Table 4 illustrates the increasing complexity of the model. Note that the simulation cases build upon each other. As the model becomes more complex by including new features, the desired modelling detail to better reflect reality increases.

5.1. Case 1: base case

In the base case, which represents a business-as-usual approach to energy storage resource provision, a battery-only storage system is considered. Also, the uncertainty associated with the forecasted time-series data is not quantified and the look-ahead energy dispatch strategy is not implemented. Specifically, the system is modelled using the expected values of the stochastic parameters. Moreover, the rule-based Greedy algorithm is run in this case, whereby the excess renewable energy generation is used to charge the battery bank before being exported to the grid. On the other hand, any load exceeding local renewable energy generation is met by discharging the battery bank before importing from the grid.

Table 5 compares the results obtained for the four simulation cases.

5.2. Case 2: incorporation of a SC bank

A comparison of the modelling results obtained for cases 1 and 2 in Table 5 indicates the following important insights:

1. The hybrid battery/SC bank reduces the cost of energy storage resource procurement by a significant ~20 % (equating to $4620), compared to the battery-only scenario. It also reduces the overall storage capacity by as much as ~31 %. The hybrid system that uses a central energy filter-based energy management strategy provides the optimal solution by leveraging the complementary characteristics of the two technologies.
2. Incorporating a SC bank into the grid-connected MG system reduces the total annual net electricity exchange cost by ~51 %. Much of the associated savings are attributable to the reduced total imported power (~63 %) during peak times when wholesale prices are higher – enabled by the increased power density of the overall storage system. Put differently, in the battery-only scenario, the storage is not able to provide transient high power densities due to its limited discharge power capacity (cycled at a C/2 rate). Accordingly, these transient power demands are imported from the national grid.

Fig. 11 presents the monthly mean 24-hour profiles for the import power and export power throughout the year in cases 1 and 2. As the figure shows, incorporating the SC bank into the system flattens the monthly mean daily import and export power profiles by addressing the transient high-power-density shortages and excesses – which are addressed by the utility grid in case 1. Not only does this generate savings from the reduced electricity imports during higher-priced hours and reduced exports during the hours on which the buyback rate is lower than the levelised cost of energy (LCOE) of the system, but it also eliminates the need for any additional power conditioning infrastructure. Yet, the total annual exported power has increased by ~7 %, which can be explained by the constraint that the MG can either import or export power at a given time-step. More specifically, reducing the need to import transient high-power-density shortages opens up the opportunity to export more excess power. Another key finding is that adding the SC bank does not have a significant impact on the temporal distribution of the power exchanges.

Additionally, Table 6 presents the descriptive statistics over 30 independent simulation runs of the MFOA. In the table, SD, RE, MAE, and RMSE respectively stand for the standard deviation, relative error, mean absolute error, and root mean square error, which can be calculated as follows:

$$SD = \sqrt{\frac{\sum_{n=1}^{N}(F_i - \overline{F})}{N-1}}, \tag{68}$$

$$RE = \frac{\sum_{n=1}^{N}(F_i - F_{best})}{F_{best}}, \tag{69}$$

$$MAE = \frac{\sum_{n=1}^{N}(F_i - F_{best})}{N}, \tag{70}$$

$$RMSE = \sqrt{\frac{\sum_{n=1}^{N}(F_i - F_{best})^2}{N}}, \tag{71}$$

where F_i represents the returned value of the objective function and the optimised values of the decision variables in the i-th independent simulation run, N is the number of runs (in this paper, $N = 30$), F_{best} is the best value of F_i obtained over the 30 independent runs, and $\overline{F}$ represents the population mean.

The resulting descriptive statistics collectively indicate that the MFOA-based solution algorithm has a robust performance, and is not sensitive to the selected initial points. There are two main reasons for this: (1) the evidenced superior efficiency of the MFOA in the integrated MG resources planning application (compared to both the conventional and other state-of-the-art meta-heuristics) [71–73], and (2) the

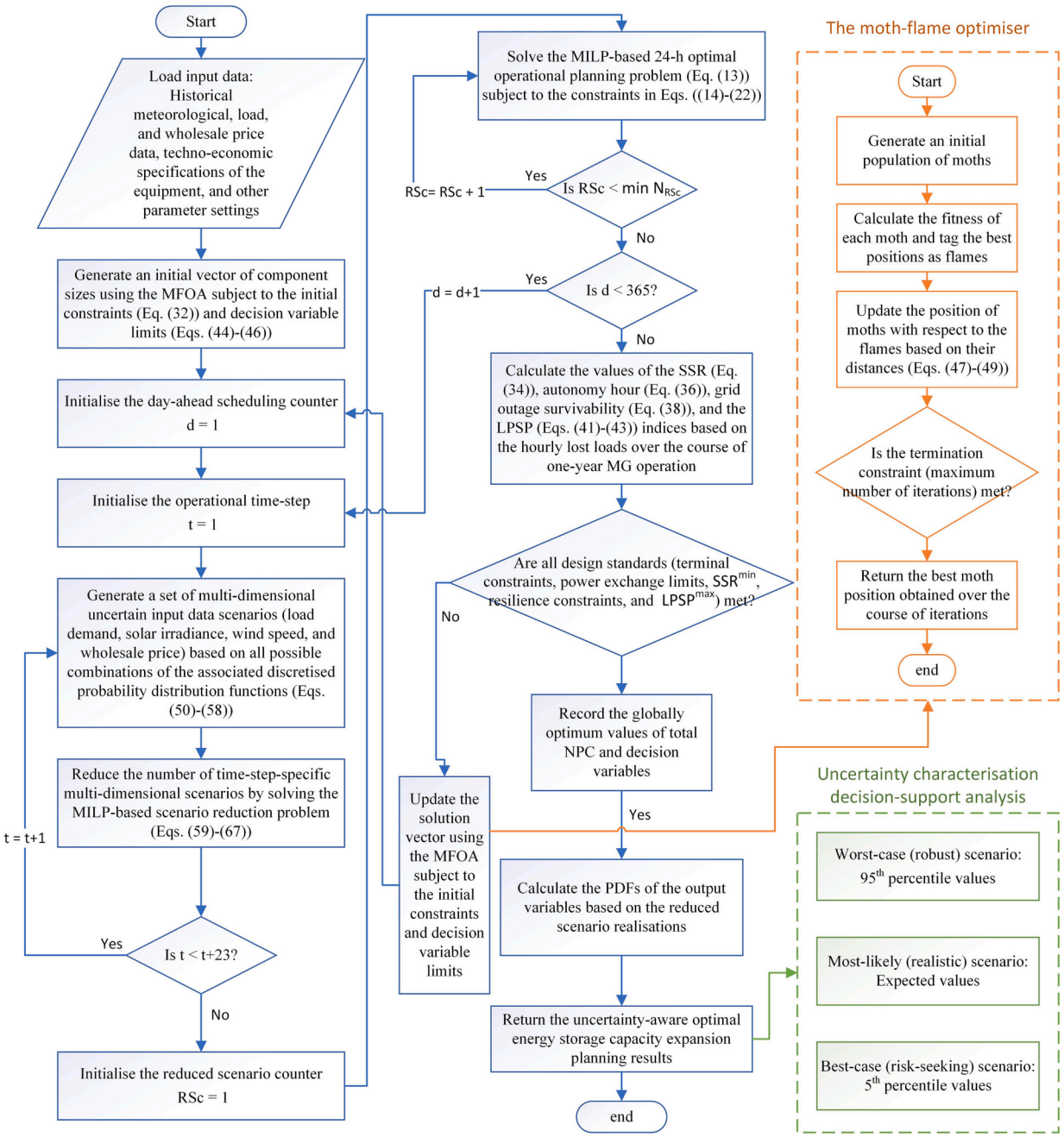

Fig. 8. Illustration of the proposed two-stage stochastic hybrid battery/SC capacity planning framework.

relatively low dimension (i.e., the number of design variables) and step size granularity (i.e., the inverse of the lengths of intervals of the candidate solutions) of the search space. Accordingly, a single run of the algorithm yields acceptable solution quality, which is used to estimate the optimal solution in the following sub-sections. Particularly, the total annual power exchanged with the upstream grid is the only contributor to the slight instability of the estimated total discounted system costs across different simulation runs.

Moreover, Fig. 12 displays the convergence process of the solution algorithm in its best- and worst-case runs. The table, additionally, compares the performance of the MFOA with the well-established meta-heuristics in the MG equipment capacity planning literature, namely the GA [111] and the PSO [112]. Accordingly, the best- and worst-case runs of the GA and the PSO (out of 30 independent runs) are presented. Two key observations can be made from Fig. 12: First, the selected number of moths (i.e., primary search agents) and the maximum number of iterations are adequate for the convergence of the solution algorithm. Second, the MFOA consistently outperforms the well-established meta-heuristics in the MG capacity planning literature. The latter observation corroborates recent work suggesting that the MFOA has particularly high efficiency in the optimal MG sizing applications [71–73].

It should also be noted that while incorporating the SC bank yields significant benefits in terms of supplementing battery power when transient high power densities are required, this paper only focuses on the steady-state operation of the system.

5.3. *Case 3: quantification of uncertainties*

In the stochastic variant of the model, the uncertain parameter-specific hourly PDFs generated based on the historical and synthetically augmented data are first approximated by dividing them into seven equal segments. The scenarios generated by different combinations of

Fig. 9. The study area: (a) the Totarabank's location on a satellite map of Aotearoa New Zealand; and (b) a satellite photograph of the site with subdivision components overlaid.
(Image courtesy of Google Earth[NZ]).

Table 2
Economic specifications of the candidate components to be integrated into the system.

Component	Nominal capacity	Capital cost	O&M cost[a]	Replacement cost[b]	Lifetime	Source
Li-ion battery (RESU 3.3, LG Chem)	3.3 kWh[c]	$3645/unit	$7.3/unit/year	$1714/unit (in year 15)	6000 cycles	[97]
EDLC SC module (XLR-48, Eaton)	166 F[d]	$1300/unit	$2.6/unit/year	$728/unit (in year 20)	1,000,000 cycles	[98]
Inverter (SPMC240-AU, Selectronic SP Pro)	3 kW	$4600/unit	$3.9/unit/year	$4600/unit	15 years	[99]

[a] Estimated based on the capital-to-O&M cost ratios presented in [100,101].
[b] Estimated based on the projections made by Goldie-Scot [102] for the Li-ion battery market, and Schmidt et al. [103] for the EDLC SC market. No considerable change is expected to the costs of power electronics devices.
[c] Energy throughput = 10.0 MWh.
[d] Energy capacity = 0.054 kWh.

Table 3
Technical specifications of the MG components.

Scalar	Value	Source	Scalar	Value	Source	Scalar	Value	Source
α_{PV}	1.64 m^2	[104]	DOD_B	88 %	[97]	$P^{max}_{ch,B}$	3 kW	[97]
$AH^{min}_{B/SC}$	12 h	–	DOD_{SC}	100 %	[98]	$P^{max}_{ch,SC}$	118 kW	[98]
b	1	[70]	$\eta_{dch,B}$	97.5 %	[97]	$P^{max}_{dch,B}$	3 kW	[97]
$cycle^{max}_B$	6000 cycles	[97]	$\eta_{dch,SC}$	98 %	[98]	$P^{max}_{dch,SC}$	118 kW	[98]
$cycle^{max}_{SC}$	1,000,000 cycles	[98]	η_I	96 %	[99]	$P_{I,ins}$	15 kW	[105]
$C_B(0)$	3.3 kWh	[97]	η_{PV}	17.4 %	[104]	Q	0.707	[105]
$C_{SC}(0)$	0.054 kWh	[98]	FiT	$0.08/kWh	[106]	$P_{I,r}$	3 kW	[104]
C^{min}_B	2.64 kWh	[97]	GOS^{min}_{MG}	8 h	–	$P_{WT,r}$	40 kWh	[107]
C^{min}_{SC}	0.043 kWh	[98]	$LPSP^{max}$	0 %	–	SSR^{min}	85 %	–
σ_B	0.3 %/day	[97]	N^{max}_B	25	–	T	8760 h	–
σ_{SC}	1.4 %/day	[98]	N^{max}_I	25	–	v_r	18.7 m/s	[107]
$\eta_{ch,B}$	97.5 %	[97]	N^{max}_{SC}	90	–	v_{ci}	3.1 m/s	[107]
$\eta_{ch,SC}$	98 %	[98]	$N_{PV,ins}$	42	[105]	v_{co}	22 m/s	[107]
Δt	1 h	–	$N_{WT,ins}$	1	[105]			

the hourly values of the uncertain inputs – obtained using the PDF discretisation – are then reduced to seven using the MILP-based scenario reduction algorithm. Accordingly, new probabilities are assigned to each of the reduced scenario vectors. For instance, Table 7 presents the value-probability pairs associated with the reduced discrete approximations for the noon hour of the day where the one-day total energy consumption is assumed to be highest, namely July 21st – the winter solstice in the Southern Hemisphere.[5] Recall that these posterior probabilities are assigned to the uncertainty vectors that contain a joint realisation of the uncertain parameters, rather than to each individual uncertain input. The corresponding parameter values in the deterministic model are as follows: solar irradiance = 400.29 W/m^2, wind speed = 6.4 m/s, load demand = 9.9 kWh, and wholesale power price = $88.1/MWh.

[5] Low-temperature heat is the main (42 %) source of household electricity demand in New Zealand, providing water heating (27 %) and space heating (15 %) [116].

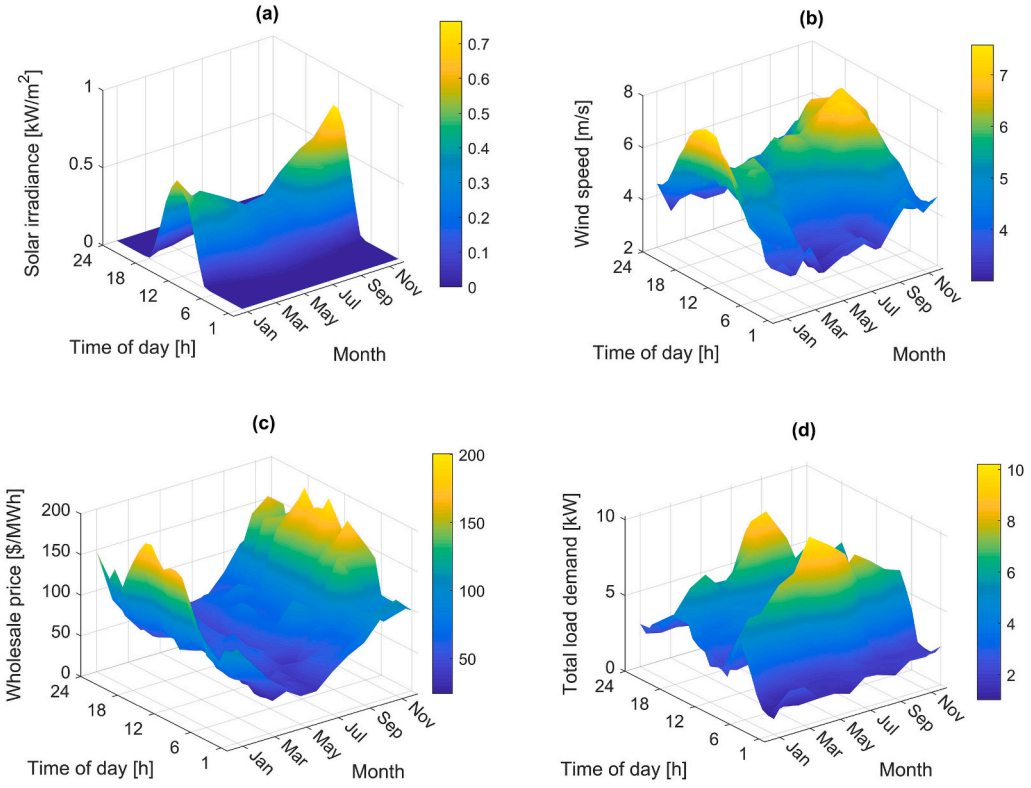

Fig. 10. Monthly mean 24-hour profile for: (a) solar irradiance; (b) wind speed; (c) wholesale power price; and (d) load power demand.

Table 4
Increasing complexity of the hybrid battery/SC capacity optimisation planning model in this paper.

Case	Incorporation of a SC bank	Characterisation of uncertainties	Day-ahead scheduling optimisation
1			
2	✓		
3	✓	✓	
4	✓	✓	✓

Table 5
Comparison of the energy storage investment planning results obtained for different simulation cases.

Model output	Case 1	Case 2	Case 3[a]	Case 4
Total NPC [$]	23,590	18,970	19,795	14,829
LCOE[b,c] [$/kWh]	0.027	0.022	0.023	0.017
Total annual net electricity exchange cost [$]	–1391	–2094	–1881	–2192
Total annual imported power [kWh]	5851	2165	2414	1258
Total annual exported power [kWh]	14,628	15,702	15,622	17,109
Total annual net energy purchased [kWh]	–8777	–13,537	–13,208	–15,851
Optimal battery bank size [kWh]	9.9	6.6	6.6	6.6
Optimal SC bank size [kWh]	N/A	0.270	0.324	0.162
Newly added inverter capacity [kW]	3	0	0	0
CPU usage time [s]	79,201	78,930	562,104	597,434

[a] The stochastic results are reported for the most-likely case, which is discussed in more detail in Section 5.3.

[b] Levelised cost of energy is defined as: $LCOE = \frac{TNPC}{\sum_{i=1}^{PL} \frac{\sum_{t=1}^{T} P_L(t)\Delta t}{(1+ir)^i}}$.

[c] Note that the calculated LCOE is only associated with the energy storage capacity procurement.

To assist the associated hybrid battery/SC expansion decision-making process, the proposed stochastic model is tailored towards different uncertainty budgets. To this end, three scenarios were considered, namely the best-case, most likely case, and worst-case scenarios. The best-case and worst-case scenarios respectively represent the 5th and 95th percentile values of the capacity planning and the associated life-cycle cost results, while the most likely case represents the expected values of the probabilistic results.

The results are assumed to follow a normal distribution. However, given the existence of only seven scenarios in the reduced stochastic simulation case, the built-in MATLAB function 'normrnd(μ,σ)' was used to generate $N = 300{,}000$ random numbers from the original population distribution X (containing the seven sets of reduced stochastic modelling results) with mean μ and standard deviation σ. Accordingly, a synthetically augmented population of $\overline{X}$ was created. The margin of error (with a confidence level of 95 %) associated with a certain output can then be obtained as follows [113]:

$$MOE = \frac{\sigma(\overline{X})}{\sqrt{N}} t_{m,N}, \tag{72}$$

where $t_{m,N}$ is the value of the variable on a t-distribution with N degrees of freedom for m% right-tailed probability corresponding to the selected uncertainty budget. For the best-case, most likely case, and worst-case scenarios, m is set to 5 %, 50 %, and 95 % respectively.

Fig. 13 presents the obtained results for the total NPC of the optimally sized HESS under different uncertainty budgets. The results are based on the optimal cost solutions estimated for the seven reduced scenarios.

Table 8 presents the comparative results for the realisation of simulation case 3 under different uncertainty budgets. The table is revealing in the following two ways:

1. Characterising the parametric uncertainties of interest may increase or decrease the expected value of the system's total NPC depending

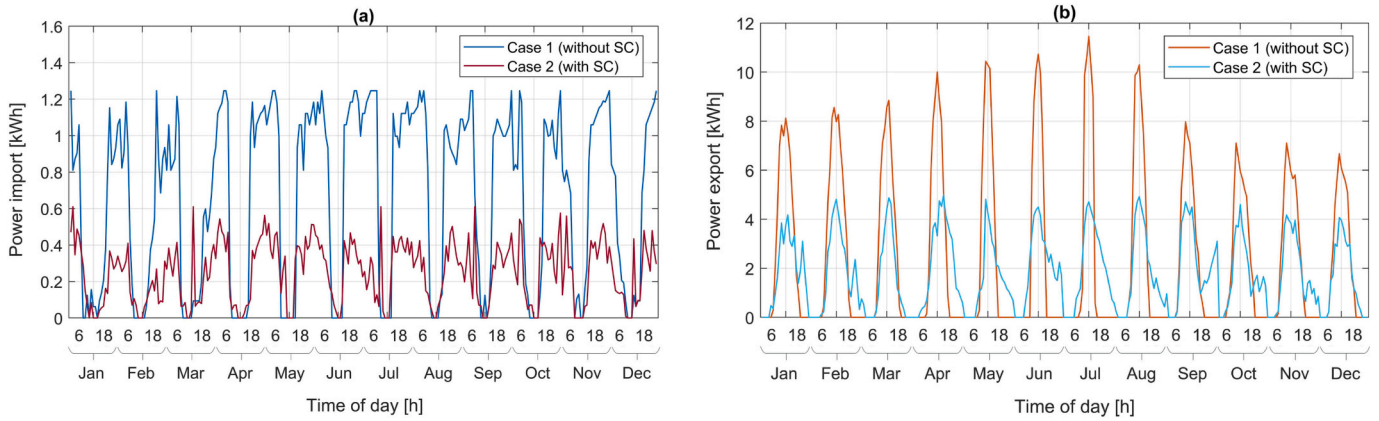

Fig. 11. Monthly mean daily profiles for the exchanged power in cases 1 and 2: (a) power import; and (b) power export. Note the change in scale in the dependent axes.

Table 6
Summary statistics of 30 independent trials of the proposed MFOA-based solution algorithm.

Output	Best	Worst	Mean	Median	SD	RE	MAE	RMSE
TNPC [$]	18,970	19,385	19,030	18,976	103.81	0.0946	59.83	327.72
LCOE [$]	0.0217	0.0222	0.0218	0.0217	1.1881×10^{-4}	0.0946	6.8482×10^{-5}	3.7509×10^{-4}
N_B [kWh]	6.60	6.60	6.60	6.60	0	0	0	0
N_{SC} [kWh]	0.27	0.27	0.27	0.27	0	0	0	0
N_I [kW]	0	0	0	0	0	0	0	0
P_{exch}[a] [kWh]	–13,537	–11,159	–13,144	–13,466	661.37	–0.8701	392.63	2150.50

[a] P_{exch} refers to the total annual net energy purchased, which is defined as: $\sum_{t=1}^{T} P_{im}(t) - P_{ex}(t)$.

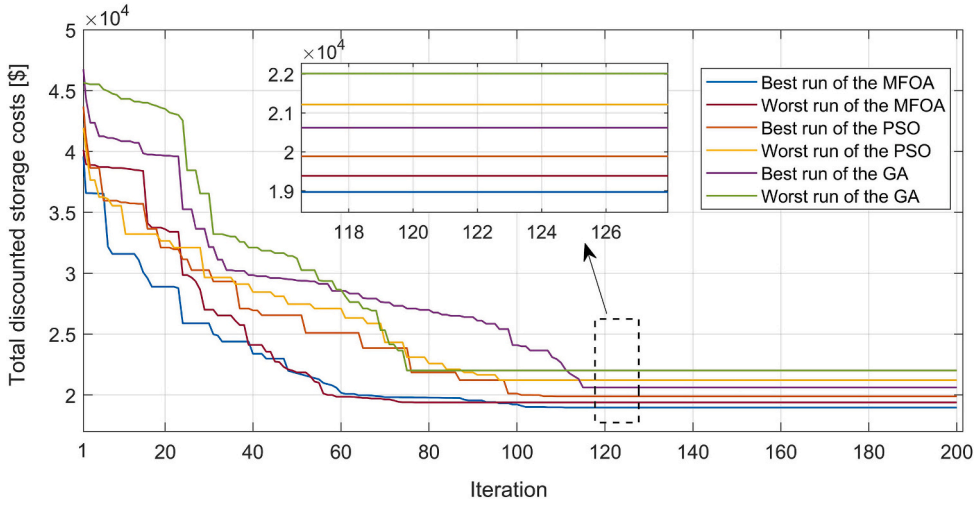

Fig. 12. Convergence of the meta-heuristic-based solution algorithm in the best and worst runs out of 30 independent trials.

on the uncertainty budget of the decision-maker. More specifically, accounting for the forecast uncertainties concerned carries a premium above the HESS's whole-life cost determined deterministically in the most likely and worst-case scenarios. The premium in the most likely and worst-case scenarios is equal to $825 (~4 %) and $6806 (~36 %), respectively. Note that the premium is primarily spent on additional SC capacity to provide a hedge against forecast uncertainties. On the other hand, the system's life-cycle cost in the highly risk-seeking scenario (best-case) can be reduced by as much as $7356 (~39 %). The savings are, in large part, attributable to the reduced overall capacity of the hybrid storage system.

2. The stochastic formulation of the model increases the CPU usage time by approximately a factor of seven. The reason is that the deterministic model is run seven times in the probabilistic model with seven (most probable and dissimilar) multi-dimensional subsets of uncertain input values. Specifically, the CPU usage time in the probabilistic model is found to be 562,104 s, which is satisfactory in the context of computationally intensive meta-heuristic-based capacity planning approaches.

The probabilistic results presented in the following sub-sections represent the most-likely case.

Table 7
Probability-value pairs for the stochastic simulation of the system for the noon hour of July 21st.

Reduced scenario	Probability of occurrence	Stochastic value of solar irradiance [W/m^2]	Stochastic value of wind speed [m/s]	Stochastic value of load demand [kWh]	Stochastic value of wholesale price [$/MWh]
1	0.2705	374.2	6.5	10.4	89.3
2	0.1953	461.4	5.9	9.5	103.2
3	0.1508	405.7	7.3	10.9	78.4
4	0.1379	358.8	5.5	10.0	67.8
5	0.1119	492.0	6.9	8.8	80.5
6	0.0966	336.9	7.1	9.3	95.1
7	0.0370	289.1	4.9	9.7	120.6

5.4. Case 4: intelligent day-ahead scheduling

This sub-section quantifies the effectiveness of the optimal scheduling of the hybrid battery/SC bank using the adopted linear programming model to look ahead over a 24-hour period, while optimally sizing the hybrid storage system. A comparison of the stochastic results with and without intelligent look-ahead provisions (cases 3 and 4), presented in Table 5, offers the following key insights:

1. Co-optimisation of the day-ahead energy scheduling and long-term investment planning of the hybrid battery/SC system reduces the total discounted system cost by a significant ~25 %, compared to the business-as-usual rule-based Greedy approach. The savings stem mainly from the added strategic foresight to look beyond a one-hour energy balance analysis. That is, optimising the storage schedules over a moving 24-hour foresight horizon (at hourly resolution), over which there is perfect foresight of the community's load demand, non-dispatchable generation, and wholesale prices, has a considerable impact on reducing the total cost of storage resource procurement – by making the decision-making process more dynamic.
2. Integrating the day-ahead linear programming-based energy scheduling optimisation model into the probabilistic optimal energy storage sizing problem increases the CPU usage time by ~6 %. More specifically, given the linearity of the optimal energy dispatch model, the standard desktop computer specified above was able to solve the daily (24-hour) energy dispatch problem in about 6 s of computational time. Accordingly, the overall year-long operational analysis solution time was found to be about 15,330 s, which was 2555 (365 days × 7 scenarios) times higher than that of a daily energy balance analysis (6 s), given that the linear programming model was run successively for every day in the baseline year under each of the reduced multi-dimensional scenarios.

Furthermore, to evaluate the impact of the energy filter's frequency response ($T_n = \frac{2\pi}{\omega_n}$) on its performance, Fig. 14 displays the monthly mean daily profiles for the SC and battery charging power for three different frequency response values, namely 6, 12, and 24. It can be seen from the figure that the higher the frequency response value, the better the energy filter performance, and the smoother the battery charging power profile. This has direct implications on the optimal design of the hybrid battery/SC system – and, in turn, on the life-cycle cost of the storage capacity expansion.

To illustrate, the optimal combination of the size of the battery and SC banks – presented as an ordered pair of their respective charging power – is found to be (9 kW, 59 kW), (6 kW, 118 kW), and (3 kW, 177 kW) respectively for the frequency response values of 6, 12, and 24 – with the associated total NPCs of $33,108 $19,795, and $26,492, respectively. Note that the change in the total NPC of the optimal capacity expansion is mainly driven by the net purchased electricity, as the changes in the NPCs associated with different combinations of the battery and SC banks – under different frequency response values of the filter – largely offset each other. As the analysis shows, there is a point at which additional SC capacity starts having a negative effect on the total NPC of the system due to excessive filtering. In this light, a trade-off frequency response value of 12 was selected in this study.

Fig. 15 shows the monthly mean daily profiles for the SOC of the Li-ion battery bank in cases 3 and 4. As the figure shows, the linear programming-based intelligent scheduling framework has successfully charged the battery bank using excess power and/or power imports during lower-priced off-peak hours to more cost-effectively meet the net load demand during peak times when wholesale prices are higher. More specifically, Fig. 15 reveals the following key insights:

1. The optimal size of the battery bank is primarily driven by the energy storage requirements during the wintertime. This is evident from the consistently high values of the battery SOC throughout the summer months (December through February).

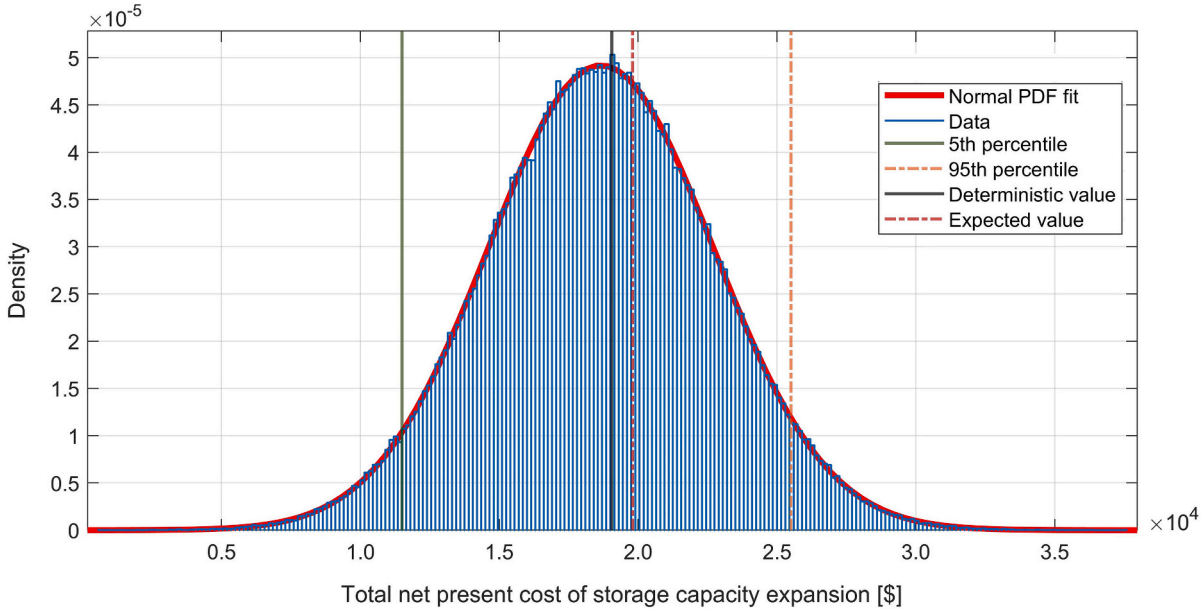

Fig. 13. Probability density function of the optimal life-cycle cost of the hybrid battery/SC bank under different uncertainty budgets.

Table 8
Comparative deterministic and stochastic results obtained under different uncertainty budgets.

Output		Case 2	Case 3 (best-case results)	Case 3 (most-likely results)	Case 3 (worst-case results)
TNPC[a] [$]		18,970	11,614	19,795	25,776
	VSS[b] [$]	N/A	7356	–825	–6806
	Relative *VSS*[b]	N/A	0.39	–0.04	–0.36
	MOE [%]	N/A	0.157	0.025	0.161
N_B [kWh]		6.6	3.3	6.6	6.6
N_{SC} [kWh]		0.27	0.216	0.324	0.486
N_I [kW]		0	0	0	0
P_{exch} [kWh]		–13,537	–10,483	–13,208	–7737
CPU usage time [s]		78,930	562,104[c]	562,104[c]	562,104[c]

[a] The *TNPC* represents the life-cycle cost of the storage capacity expansion.
[b] The *VSS* stands for the value of the stochastic solution, which is defined as the optimal deterministic solution minus the optimal stochastic solution. The relative *VSS* is defined as the *VSS* divided by the optimal deterministic solution [114].
[c] Note that the CPU usage time associated with case 3 represents the time required to simulate the seven reduced scenario vectors. The best-, most likely-, and worst-case analyses are then made based on the results obtained for these seven sets of inputs.

2. The minimum daily battery SOC often occurs during the morning (6 a.m. to 10 a.m.) and evening (5 p.m. to 9 p.m.) peak hours when the MG peak coincides with the utility grid peak. On the other hand, the charging periods are efficiently scheduled to when prices are lowest.
3. The intelligent scheduling design strategy (case 4) has effectively reduced the peak-to-average ratio of the monthly energy content profiles – which drives capacity reductions. This is achieved in light of the optimisation-based energy management framework's strategic foresight of the daily load demand, local generation, and wholesale prices at hourly resolution – contrary to the rule-based Greedy energy management framework's fixed approach. Consequently, the average charge/discharge schedules of the battery bank are considerably different in the two cases. For instance, the rate of the battery charging during the light-load hours of 0:00 a.m. to 4:00 a.m. in July is higher in case 4, with the difference coming from the utility grid to more cost-effectively meet the load demand in the remaining hours of the day. Then, during the 5th and 6th hours, despite the shortage of local generation, the intelligent dispatch strategy continues charging the battery because of the lower wholesale price values than the LCOE of the capacity expansion. On the other hand, despite the excess power, the intelligent scheduling framework discharges the battery bank for export during the 9th and 10th hours. This can be explained as follows. Given the fixed feed-in-tariff, the daily forecasts of wholesale prices, and the inability of the storage to be charged and discharged simultaneously (which makes battery charging during the off-peak, lower-priced hours more economically viable), it is cost-optimal for the MG to export the excess power stored during the off-peak hours at these time-steps.

5.5. Sensitivity analysis: economics of energy arbitrage

To analyse the impact of the variations in the feed-in-tariff and the battery capital cost on the optimal combination of the storage components and the exchanged power with the grid, Table 9 details the cost-optimal solutions obtained for three cases, namely: the existing situation, a realistic projection case (where the feed-in-tariff is increased to $0.18/kWh and the battery capital cost is reduced by 40 %), and an extreme case (where the feed-in-tariff is increased to $0.43/kWh[6] and the battery capital cost is reduced by 70 %).

As can be seen from Table 9, a further battery capacity of 9.9 kWh and a further inverter capacity of 3 kW have been allocated for arbitraging on electricity tariffs under the realistic projection case scenario, which increase to 75.9 kWh and 12 kW under the extreme case scenario, respectively. Accordingly, defining the internal rate of return (IRR) as the discount rate at which the status quo (no-storage case) and the expanded system have the same total NPC, the IRR of the storage

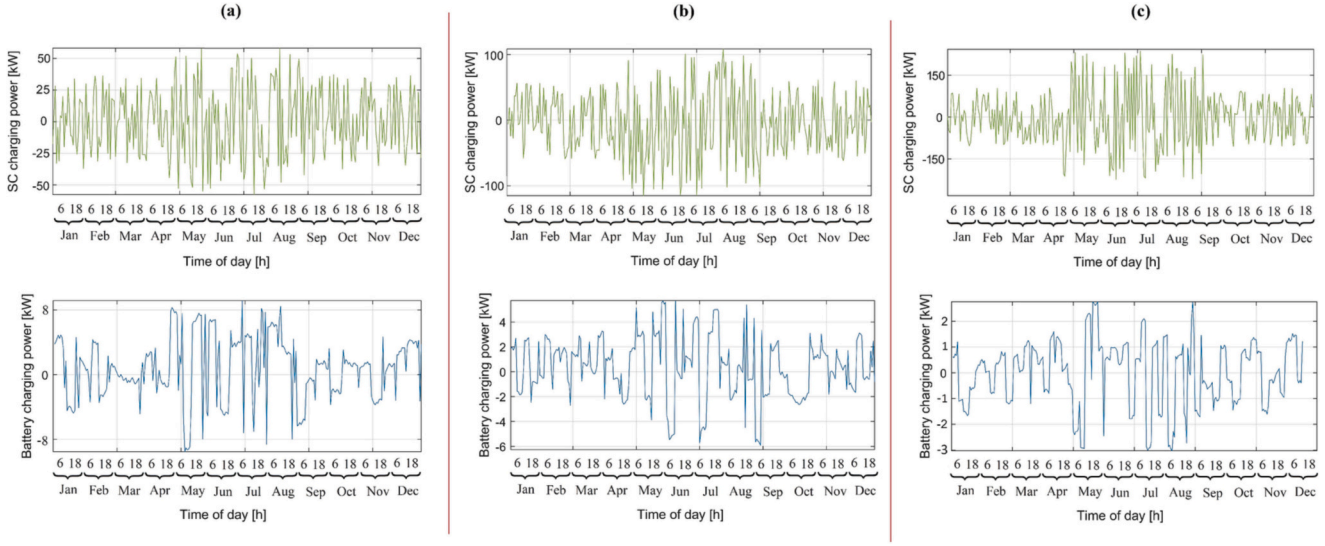

Fig. 14. Monthly mean daily profiles for the SC and battery charging power under different frequency response values: (a) $T_n = 6$, $T_n = 12$, and $T_n = 24$. Note the change in scale in the dependent axes.

[6] Considering income streams such as the frequency control ancillary services, operating reserve, and network support markets.

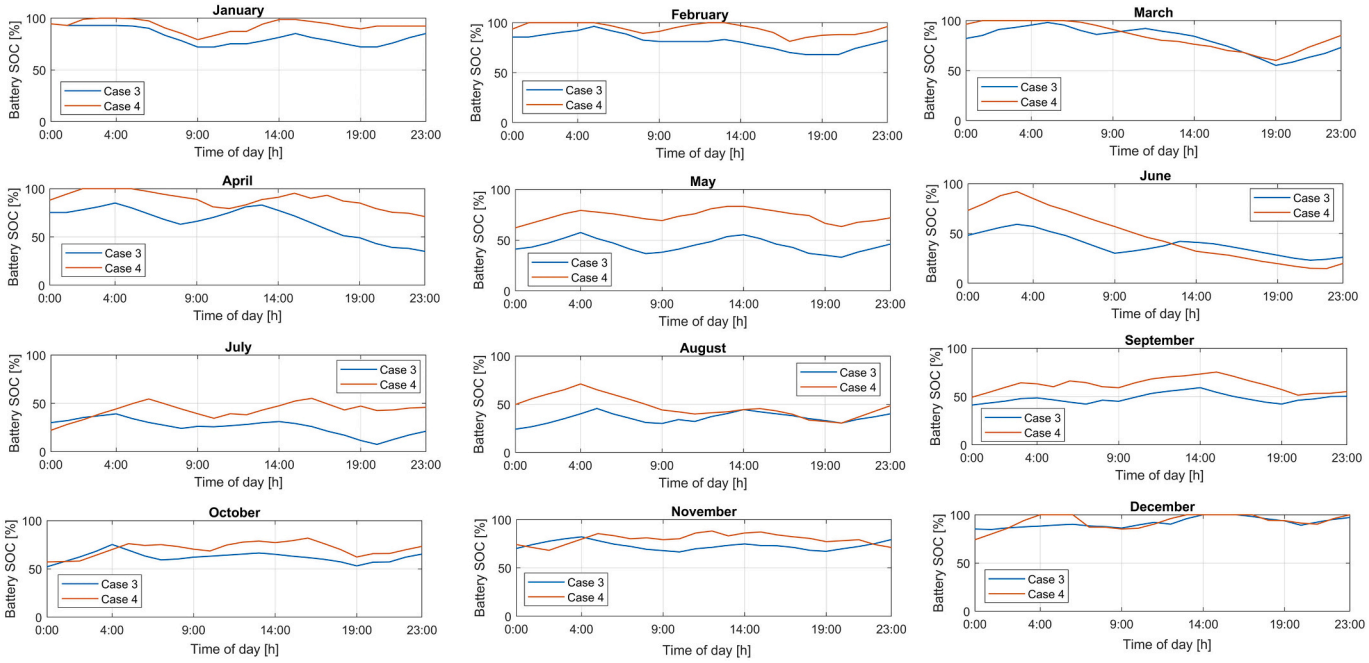

Fig. 15. Monthly mean daily profiles for the energy content of the hybrid battery/SC bank in cases 3 and 4.

Table 9
Detailed modelling results under the existing situation, realistic projection case, and extreme case scenarios.

Model output	Existing situation	Realistic projection	Extreme case
Total NPC [$]	19,795	7120	–63,205
Internal rate of return [%]	16.83	53.14	235.90
Total annual net electricity exchange cost [$]	–1881	–3514	–13,992
Total annual net energy arbitrage trade [kWh]	0	10,211	30,054
Total annual imported power [kWh]	2414	12,625	32,468
Total annual exported power [kWh]	15,622	24,143	40,403
Total annual net energy purchased [kWh]	–13,208	–11,518	–7935
Optimal battery bank size [kWh]	6.6	16.5	82.5
Optimal SC bank size [kWh]	0.324	0.324	0.324
Newly added inverter capacity [kW]	0	3	12

capacity expansion is increased to ~53 % and ~236 % in the realistic projection and extreme case scenarios from ~17 % in the existing situation scenario.

Additionally, Table 9 indicates that as the feed-in-tariff increases and/or the battery capital cost decreases, the total net energy purchased in the optimal solution increases, while adhering to the minimum required SSR. The underlying reason for this observation is that the increased optimal battery capacity – as a result of reaching arbitrage profitability – increases the opportunity to store the off-peak energy purchased from the grid – at costs lower than the system's LCOE – for later on-site use, to cost-optimally supplement the power generated by onsite non-dispatchable renewables.

6. Conclusions and future work

Hybridising different energy storage technologies tailored to operating on different time scales is increasingly recognised as one of the most cost-effective ways of accommodating the variability and limited predictability of renewable energy sources – a prerequisite for integrating significant volumes of DERs into the grid. This paper has presented a novel, meta-heuristic-based two-stage stochastic model for the nested capacity planning and energy scheduling co-optimisation of hybrid battery/SC energy storage systems to be integrated into grid-connected MGs.

Based on the numeric simulation results obtained for the case of Totarabank Subdivision, in Aotearoa New Zealand, the following main quantifiable findings emerge from this study:

- Significant cost reduction with super-capacitor integration: The addition of a SC bank to a battery-supported MG significantly reduces the total energy throughput of the battery bank and effectively mitigates the stresses induced by high charge/discharge rate responses. By leveraging the energy filter concept, it has been demonstrated that a battery/SC hybrid energy storage system can reduce the total discounted cost associated with adding capital-intensive storage resources to an on-grid MG by as much as approximately ~20 %. This reduction is achieved by smoothing power fluctuations in and out of the battery bank, thus extending its lifespan.
- Importance of probabilistic modelling: Introducing a probabilistic dimension to meta-heuristic-based optimal storage capacity planning models tailored to hybrid battery/SC systems is essential. The comparison of stochastic and deterministic variants of the proposed model reveals that failure to quantify the most salient model-inherent parametric uncertainties results in a significant underestimation of total discounted system costs. Specifically, in the most-likely case and worst-case scenarios, underestimations of approximately 4 % and 36 % have been observed, respectively. Furthermore, the best-case stochastic results are found to be at least 39 % lower than deterministic results. The developed stochastic model effectively accommodates various sources of uncertainty while maintaining acceptable computational efficiency.
- Energy management optimisation: Utilising an intelligent scheduling design framework with 24-hour look-ahead periods for the dispatch of hybrid battery/SC systems integrated into grid-connected MGs can significantly reduce the total life-cycle cost of the HESS, up to

approximately 25 % when compared to a rule-based Greedy energy dispatch strategy. This approach optimally utilises the available energy resources, resulting in cost savings.

- Economic viability and sensitivity analysis: At the existing average buyback rate of $0.08/kWh in Aotearoa New Zealand, it has been found that the potential investment in a hybrid battery/SC system for arbitrage alone is not economically viable. This conclusion holds even when considering lower C-rated behind-the-meter batteries, which are unable to effectively track the volatility of the spot market. Additionally, a sensitivity analysis has demonstrated the robustness of this finding to increased buyback rates, up to at least $0.23/kWh, at current Li-ion battery technology costs.

While this study provides valuable insights, it is important to acknowledge that the results are limited by certain assumptions made in setting the techno-economic parameters, which were held fixed. Future research endeavours should aim to further characterise the uncertainty associated with techno-economic data, such as battery and SC bank replacement costs and lifetimes, to improve the robustness of hybrid energy storage capacity planning approaches. Copula theory may offer a viable, less computationally expensive method for achieving this goal by deriving a multivariate joint distribution of uncertain variables.

The insights gained from our study not only highlight the effectiveness of hybrid battery/SC systems in improving the resilience and cost-effectiveness of renewable energy integration within the context of the selected case study in Aotearoa New Zealand, but also suggest their scalability and applicability in diverse global micro-grid settings.

In conclusion, this research has advanced the understanding of grid-connected hybrid energy storage systems, providing a comprehensive framework that combines capacity planning and optimal scheduling. The findings underscore the potential of hybridisation, the importance of probabilistic modelling, and the significance of intelligent energy management. These insights contribute to the ongoing evolution of sustainable energy integration strategies in modern micro-grid systems.

CRediT authorship contribution statement

Soheil Mohseni: Conceptualization, Methodology, Data curation, Formal analysis, Investigation, Resources, Software, Validation, Visualization, Writing – original draft. **Alan C. Brent:** Supervision, Project administration, Formal analysis, Investigation, Resources, Validation, Writing – review & editing.

Declaration of competing interest

The authors declare that they have no known competing financial interests or personal relationships that could have appeared to influence the work reported in this paper.

Data availability

Data will be made available on request.

Appendix A

Fig. A1 shows power rating versus rated energy capacity for energy storage technologies that have been deployed at significant scale across time scales ranging from fractions of a second to many hours [27]. The figure additionally presents the nominal duration of discharge at the corresponding rated power of the energy storage technologies.

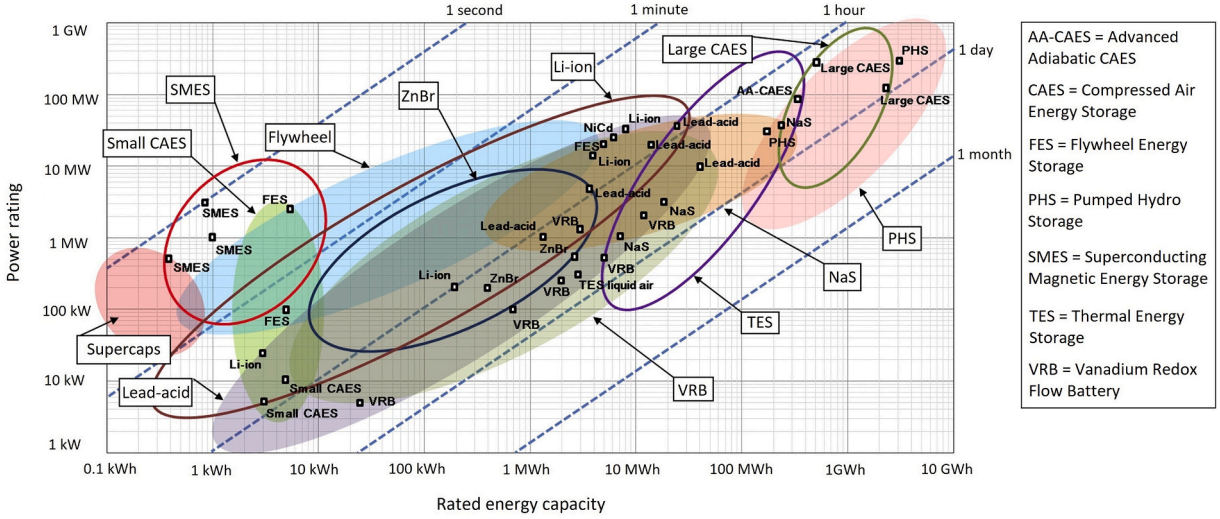

Fig. A1. Power rating versus rated energy capacity for various grid-supporting energy storage technologies. (Adapted from [27]).

In the area of hybrid energy storage systems, the intricate interplay between power rating and rated energy capacity of the constituent components, particularly Li-ion batteries and EDLC super-capacitors, assumes paramount significance. Li-ion batteries are renowned for their ability to provide stable, prolonged energy storage owing to their substantial rated energy capacity. Conversely, EDLC super-capacitors boast a strong power rating, which allows for rapid energy discharge. It is the synergy between these divergent characteristics that accentuates the overall performance of hybrid storage. The Li-ion battery, with its elevated energy reservoir, caters to the extended energy requirements, ensuring system stability over extended durations, while the high power rating of EDLC super-capacitors facilitates instantaneous energy delivery during abrupt power surges. This collaborative dynamic strikes an equilibrium in energy management, averting undue strain on Li-ion batteries during sudden power fluctuations – thereby, improving the overall efficiency and longevity of the energy storage system. Thus, this harmonious partnership between power rating and rated energy capacity encapsulates a pivotal dimension of hybrid storage design and operation, with ramifications extending to various applications within the broader domain of resilient and cost-effective energy grid integration.

References

[1] O. Walter, A. Tremel, M. Prenzel, S. Becker, J. Schaefer, Techno-economic analysis of hybrid energy storage concepts via flowsheet simulations, cost modeling and energy system design, Energy Convers. Manag. 218 (2020) 112955.

[2] J. Tobajas, F. Garcia-Torres, P. Roncero-Sánchez, J. Vázquez, L. Bellatreche, E. Nieto, Resilience-oriented schedule of microgrids with hybrid energy storage system using model predictive control, Appl. Energy 306 (2022) 118092.

[3] X. Wang, J. Zhou, B. Qin, L. Guo, Coordinated control of wind turbine and hybrid energy storage system based on multi-agent deep reinforcement learning for wind power smoothing, J. Energy Storage 57 (2023) 106297.

[4] E. Akbari, S.F. Mousavi Shabestari, S. Pirouzi, M. Jadidoleslam, Network flexibility regulation by renewable energy hubs using flexibility pricing-based energy management, Renew. Energy 206 (2023) 295–308.

[5] L. Al-Ghussain, A. Darwish Ahmad, A.M. Abubaker, M.A. Mohamed, An integrated photovoltaic/wind/biomass and hybrid energy storage systems towards 100% renewable energy microgrids in university campuses, Sustain. Energy Technol. Assess. 46 (2021) 101273.

[6] X. Lin, R. Zamora, Controls of hybrid energy storage systems in microgrids: critical review, case study and future trends, J. Energy Storage 47 (2022) 103884.

[7] M.R. Jokar, S. Shahmoradi, A.H. Mohammed, L.K. Foong, B.N. Le, S. Pirouzi, Stationary and mobile storages-based renewable off-grid system planning considering storage degradation cost based on information-gap decision theory optimization, J. Energy Storage 58 (2023) 106389.

[8] O. Ogunmodede, K. Anderson, D. Cutler, A. Newman, Optimizing design and dispatch of a renewable energy system, Appl. Energy 287 (2021) 116527.

[9] U. Damisa, N.I. Nwulu, Y. Sun, A robust energy and reserve dispatch model for prosumer microgrids incorporating demand response aggregators, J. Renew. Sustain. Energy 10 (5) (2018) 55301.

[10] G. Piltan, S. Pirouzi, A. Azarhooshang, A. Rezaee Jordehi, A. Paeizi, M. Ghadamyari, Storage-integrated virtual power plants for resiliency enhancement of smart distribution systems, J. Energy Storage 55 (2022) 105563.

[11] X. Yang, Z. Chen, X. Huang, R. Li, S. Xu, C. Yang, Robust capacity optimization methods for integrated energy systems considering demand response and thermal comfort, Energy 221 (2021) 119727.

[12] J. Wang, K.-J. Li, Y. Liang, Z. Javid, Optimization of multi-energy microgrid operation in the presence of PV, heterogeneous energy storage and integrated demand response, Appl. Sci. 11 (3) (2021).

[13] A.M. Jasim, B.H. Jasim, S. Mohseni, A.C. Brent, Consensus-based dispatch optimization of a microgrid considering meta-heuristic-based demand response scheduling and network packet loss characterization, Energy AI 11 (2023) 100212.

[14] A. Pirouzi, J. Aghaei, S. Pirouzi, V. Vahidinasab, A.R. Jordehi, Exploring potential storage-based flexibility gains of electric vehicles in smart distribution grids, J. Energy Storage 52 (2022) 105056.

[15] A. Dini, A. Hassankashi, S. Pirouzi, M. Lehtonen, B. Arandian, A.A. Baziar, A flexible-reliable operation optimization model of the networked energy hubs with distributed generations, energy storage systems and demand response, Energy 239 (2022) 121923.

[16] M.M. Mohamed, H.M. El Zoghby, S.M. Sharaf, M.A. Mosa, Optimal virtual synchronous generator control of battery/supercapacitor hybrid energy storage system for frequency response enhancement of photovoltaic/diesel microgrid, J. Energy Storage 51 (2022) 104317.

[17] S. Kotra, M.K. Mishra, Design and stability analysis of DC microgrid with hybrid energy storage system, IEEE Trans. Sustain. Energy 10 (3) (2019) 1603–1612.

[18] T.B. Nkwanyana, M.W. Siti, Z. Wang, I. Toudjeu, N.T. Mbungu, W. Mulumba, An assessment of hybrid-energy storage systems in the renewable environments, J. Energy Storage 72 (2023) 108307.

[19] M. Taghizadeh, S. Bahramara, F. Adabi, S. Nojavan, Optimal operation of storage-based hybrid energy system considering market price uncertainty and peak demand management, J. Energy Storage 30 (2020) 101519.

[20] A. Alahyari, M. Ehsan, M. Mousavizadeh, A hybrid storage-wind virtual power plant (VPP) participation in the electricity markets: a self-scheduling optimization considering price, renewable generation, and electric vehicles uncertainties, J. Energy Storage 25 (2019) 100812.

[21] T.S. Babu, K.R. Vasudevan, V.K. Ramachandaramurthy, S.B. Sani, S. Chemud, R. M. Lajim, A comprehensive review of hybrid energy storage systems: converter topologies, control strategies and future prospects, IEEE Access 8 (2020) 148702–148721.

[22] R. Hemmati, H. Saboori, Emergence of hybrid energy storage systems in renewable energy and transport applications – a review, Renew. Sust. Energ. Rev. 65 (2016) 11–23.

[23] X. Zhang, X. Yu, X. Ye, S. Pirouzi, Economic energy management of networked flexi-renewable energy hubs according to uncertainty modeling by the unscented transformation method, Energy 278 (2023) 128054.

[24] Z. Yan, Y. Zhang, R. Liang, W. Jin, An allocative method of hybrid electrical and thermal energy storage capacity for load shifting based on seasonal difference in district energy planning, Energy 207 (2020) 118139.

[25] Y. Wang, et al., Research on capacity planning and optimization of regional integrated energy system based on hybrid energy storage system, Appl. Therm. Eng. 180 (2020) 115834.

[26] A.S. Jacob, R. Banerjee, P.C. Ghosh, Sizing of hybrid energy storage system for a PV based microgrid through design space approach, Appl. Energy 212 (2018) 640–653.

[27] X. Luo, J. Wang, M. Dooner, J. Clarke, Overview of current development in electrical energy storage technologies and the application potential in power system operation, Appl. Energy 137 (2015) 511–536.

[28] N.T. Mbungu, A.A. Ismail, M. AlShabi, R.C. Bansal, A. Elnady, A.K. Hamid, Control and estimation techniques applied to smart microgrids: a review, Renew. Sust. Energ. Rev. 179 (2023) 113251.

[29] S. Hajiaghasi, A. Salemnia, M. Hamzeh, Hybrid energy storage system for microgrids applications: a review, J. Energy Storage 21 (2019) 543–570.

[30] R. Xiong, H. Chen, C. Wang, F. Sun, Towards a smarter hybrid energy storage system based on battery and ultracapacitor - a critical review on topology and energy management, J. Clean. Prod. 202 (2018) 1228–1240.

[31] A. Bharatee, P.K. Ray, B. Subudhi, A. Ghosh, Power management strategies in a hybrid energy storage system integrated AC/DC microgrid: a review, Energies 15 (19) (2022).

[32] S. Choudhury, Review of energy storage system technologies integration to microgrid: types, control strategies, issues, and future prospects, J. Energy Storage 48 (2022) 103966.

[33] S. Günther, L. Weber, A.L. Bensmann, R. Hanke-Rauschenbach, Structured analysis and review of filter-based control strategies for hybrid energy storage systems, IEEE Access 10 (2022) 126269–126284.

[34] C.-H. Li, X.-J. Zhu, G.-Y. Cao, S. Sui, M.-R. Hu, Dynamic modeling and sizing optimization of stand-alone photovoltaic power systems using hybrid energy storage technology, Renew. Energy 34 (3) (2009) 815–826.

[35] T. Zhou, W. Sun, Optimization of battery–supercapacitor hybrid energy storage station in wind/solar generation system, IEEE Trans. Sustain. Energy 5 (2) (2014) 408–415.

[36] H. Jia, Y. Mu, Y. Qi, A statistical model to determine the capacity of battery–supercapacitor hybrid energy storage system in autonomous microgrid, Int. J. Electr. Power Energy Syst. 54 (2014) 516–524.

[37] Z. Song, et al., Multi-objective optimization of a semi-active battery/supercapacitor energy storage system for electric vehicles, Appl. Energy 135 (2014) 212–224.

[38] S. Mohammadi, A. Mohammadi, Stochastic scenario-based model and investigating size of battery energy storage and thermal energy storage for micro-grid, Int. J. Electr. Power Energy Syst. 61 (2014) 531–546.

[39] I. Janghorban Esfahani, S. Lee, C. Yoo, Extended-power pinch analysis (EPoPA) for integration of renewable energy systems with battery/hydrogen storages, Renew. Energy 80 (2015) 1–14.

[40] S. Wogrin, D.F. Gayme, Optimizing storage siting, sizing, and technology portfolios in transmission-constrained networks, IEEE Trans. Power Syst. 30 (6) (2015) 3304–3313.

[41] P. Zhao, J. Wang, Y. Dai, Capacity allocation of a hybrid energy storage system for power system peak shaving at high wind power penetration level, Renew. Energy 75 (2015) 541–549.

[42] X. Wang, A. Palazoglu, N.H. El-Farra, Operational optimization and demand response of hybrid renewable energy systems, Appl. Energy 143 (2015) 324–335.

[43] Y. Zhang, X. Tang, Z. Qi, Z. Liu, The Ragone plots guided sizing of hybrid storage system for taming the wind power, Int. J. Electr. Power Energy Syst. 65 (2015) 246–253.

[44] S. Bae, S.U. Jeon, J.-W. Park, A study on optimal sizing and control for hybrid energy storage system with SMES and battery, IFAC-PapersOnLine 48 (30) (2015) 507–511.

[45] W. Dong, Y. Li, J. Xiang, Optimal sizing of a stand-alone hybrid power system based on battery/hydrogen with an improved ant colony optimization, Energies 9 (10) (2016) 785.

[46] H. Shahinzadeh, M. Moazzami, S.H. Fathi, G.B. Gharehpetian, Optimal sizing and energy management of a grid-connected microgrid using HOMER software, in: 2016 Smart Grids Conference (SGC), 2016, pp. 1–6.

[47] Y. Liu, W. Du, L. Xiao, H. Wang, S. Bu, J. Cao, Sizing a hybrid energy storage system for maintaining power balance of an isolated system with high penetration of wind generation, IEEE Trans. Power Syst. 31 (4) (2016) 3267–3275.

[48] Y. Ghiassi-Farrokhfal, C. Rosenberg, S. Keshav, M.-B. Adjaho, Joint optimal design and operation of hybrid energy storage systems, IEEE J. Sel. Areas Commun. 34 (3) (2016) 639–650.

[49] S. Sukumar, H. Mokhlis, S. Mekhilef, K. Naidu, M. Karimi, Mix-mode energy management strategy and battery sizing for economic operation of grid-tied microgrid, Energy 118 (2017) 1322–1333.

[50] B. Li, R. Roche, D. Paire, A. Miraoui, Sizing of a stand-alone microgrid considering electric power, cooling/heating, hydrogen loads and hydrogen storage degradation, Appl. Energy 205 (2017) 1244–1259.

[51] S. Mashayekh, M. Stadler, G. Cardoso, M. Heleno, A mixed integer linear programming approach for optimal DER portfolio, sizing, and placement in multi-energy microgrids, Appl. Energy 187 (2017) 154–168.

[52] I. Aldaouab, M. Daniels, Microgrid battery and thermal storage for improved renewable penetration and curtailment, in: 2017 International Energy and Sustainability Conference (IESC), 2017, pp. 1–5.

[53] A. Abdelkader, A. Rabeh, D. Mohamed Ali, J. Mohamed, Multi-objective genetic algorithm based sizing optimization of a stand-alone wind/PV power supply system with enhanced battery/supercapacitor hybrid energy storage, Energy 163 (2018) 351–363.

[54] A. Abbassi, M.A. Dami, M. Jemli, A statistical approach for hybrid energy storage system sizing based on capacity distributions in an autonomous PV/wind power generation system, Renew. Energy 103 (2017) 81–93.

[55] X. Feng, J. Gu, X. Guan, Optimal allocation of hybrid energy storage for microgrids based on multi-attribute utility theory, J. Mod. Power Syst. Clean Energy 6 (1) (2018) 107–117.

[56] U. Akram, M. Khalid, S. Shafiq, An innovative hybrid wind-solar and battery-supercapacitor microgrid system—development and optimization, IEEE Access 5 (2017) 25897–25912.
[57] S. Günther, A. Bensmann, R. Hanke-Rauschenbach, Theoretical dimensioning and sizing limits of hybrid energy storage systems, Appl. Energy 210 (2018) 127–137.
[58] F. Xu, J. Liu, S. Lin, Q. Dai, C. Li, A multi-objective optimization model of hybrid energy storage system for non-grid-connected wind power: a case study in China, Energy 163 (2018) 585–603.
[59] J. Cao, W. Du, H. Wang, M. McCulloch, Optimal sizing and control strategies for hybrid storage system as limited by grid frequency deviations, IEEE Trans. Power Syst. 33 (5) (2018) 5486–5495.
[60] P. Nagapurkar, J.D. Smith, Techno-economic optimization and environmental life cycle assessment (LCA) of microgrids located in the US using genetic algorithm, Energy Convers. Manag. 181 (2019) 272–291.
[61] A. Lorestani, G.B. Gharehpetian, M.H. Nazari, Optimal sizing and techno-economic analysis of energy- and cost-efficient standalone multi-carrier microgrid, Energy 178 (2019) 751–764.
[62] Y. Jiang, L. Kang, Y. Liu, A unified model to optimize configuration of battery energy storage systems with multiple types of batteries, Energy 176 (2019) 552–560.
[63] D.N. Luta, A.K. Raji, Decision-making between a grid extension and a rural renewable off-grid system with hydrogen generation, Int. J. Hydrog. Energy 43 (20) (2018) 9535–9548.
[64] H. Chen, Z. Zhang, C. Guan, H. Gao, Optimization of sizing and frequency control in battery/supercapacitor hybrid energy storage system for fuel cell ship, Energy 197 (2020) 117285.
[65] T. Zhu, R. Lot, R.G.A. Wills, X. Yan, Sizing a battery-supercapacitor energy storage system with battery degradation consideration for high-performance electric vehicles, Energy 208 (2020) 118336.
[66] B. Yang, et al., Design and implementation of battery/SMES hybrid energy storage systems used in electric vehicles: a nonlinear robust fractional-order control approach, Energy 191 (2020) 116510.
[67] K. Uddin, S. Perera, W.D. Widanage, L. Somerville, J. Marco, Characterising lithium-ion battery degradation through the identification and tracking of electrochemical battery model parameters, Batteries 2 (2) (2016) 13.
[68] Y. Liu, X. Wu, J. Du, Z. Song, G. Wu, Optimal sizing of a wind-energy storage system considering battery life, Renew. Energy 147 (2020) 2470–2483.
[69] L. Xu, X. Ruan, C. Mao, B. Zhang, Y. Luo, An improved optimal sizing method for wind-solar-battery hybrid power system, IEEE Trans. Sustain. Energy 4 (3) (2013) 774–785.
[70] S. Mirjalili, Moth-flame optimization algorithm: a novel nature-inspired heuristic paradigm, Knowl.-Based Syst. 89 (2015) 228–249.
[71] S. Mohseni, A.C. Brent, Economic viability assessment of sustainable hydrogen production, storage, and utilisation technologies integrated into on- and off-grid micro-grids: a performance comparison of different meta-heuristics, Int. J. Hydrog. Energy 45 (59) (2020) 34412–34436.
[72] S. Mohseni, R. Khalid, A.C. Brent, Metaheuristic-based isolated microgrid sizing and uncertainty quantification considering EVs as shiftable loads, Energy Rep. 8 (2022) 11288–11308.
[73] S. Mohseni, A.C. Brent, D. Burmester, A demand response-centred approach to the long-term equipment capacity planning of grid-independent micro-grids optimized by the moth-flame optimization algorithm, Energy Convers. Manag. 200 (2019) 112105.
[74] S. Diaf, D. Diaf, M. Belhamel, M. Haddadi, A. Louche, A methodology for optimal sizing of autonomous hybrid PV/wind system, Energy Policy 35 (11) (2007) 5708–5718.
[75] M. Mohammadi, S.H. Hosseinian, G.B. Gharehpetian, Optimization of hybrid solar energy sources/wind turbine systems integrated to utility grids as microgrid (MG) under pool/bilateral/hybrid electricity market using PSO, Sol. Energy 86 (1) (2012) 112–125.
[76] Y.-L. Lee, T. Tjhung, Rainflow cycle counting techniques, in: Metal Fatigue Analysis Handbook: Practical Problem-solving Techniques for Computer-aided Engineering vol. 89, 2011.
[77] Y. Shi, B. Xu, Y. Tan, B. Zhang, A convex cycle-based degradation model for battery energy storage planning and operation, in: 2018 Annual American Control Conference (ACC), IEEE, 2018, pp. 4590–4596.
[78] MathWorks®, Rainflow counts for fatigue analysis [Online]. Available, https://au.mathworks.com/help/signal/ref/rainflow.html (Accessed: 23-Feb-2023).
[79] J. Li, A.M. Gee, M. Zhang, W. Yuan, Analysis of battery lifetime extension in a SMES-battery hybrid energy storage system using a novel battery lifetime model, Energy 86 (2015) 175–185.
[80] A.J. Pimm, J. Palczewski, R. Morris, T.T. Cockerill, P.G. Taylor, Community energy storage: a case study in the UK using a linear programming method, Energy Convers. Manag. 205 (2020) 112388.
[81] A. Soto, A. Berrueta, M. Mateos, P. Sanchis, A. Ursúa, Impact of micro-cycles on the lifetime of lithium-ion batteries: an experimental study, J. Energy Storage 55 (2022) 105343.
[82] B.K. Kim, S. Sy, A. Yu, J. Zhang, Electrochemical supercapacitors for energy storage and conversion, in: Handbook of Clean Energy Systems, 2015, pp. 1–25.
[83] O. Hafez, K. Bhattacharya, Optimal planning and design of a renewable energy based supply system for microgrids, Renew. Energy 45 (2012) 7–15.
[84] S. Mohseni, A.C. Brent, D. Burmester, A sustainable energy investment planning model based on the micro-grid concept using recent metaheuristic optimization algorithms, in: 2019 IEEE Congress on Evolutionary Computation (CEC), 2019, pp. 219–226.
[85] D. Akinyele, Techno-economic and Life-cycle Impact Analysis of Solar Photovoltaic Microgrid Systems for Off-grid Communities (PhD thesis), Victoria University of Wellington, 2016.
[86] Y. Zhang, A. Lundblad, P.E. Campana, F. Benavente, J. Yan, Battery sizing and rule-based operation of grid-connected photovoltaic-battery system: a case study in Sweden, Energy Convers. Manag. 133 (2017) 249–263.
[87] T. Ma, H. Yang, L. Lu, A feasibility study of a stand-alone hybrid solar–wind–battery system for a remote island, Appl. Energy 121 (2014) 149–158.
[88] E. Ofry, A. Braunstein, The loss of power supply probability as a technique for designing stand-alone solar electrical (photovoltaic) systems, IEEE Power Eng. Rev. PER-3 (5) (1983) 34–35.
[89] F. McLoughlin, A. Duffy, M. Conlon, The generation of domestic electricity load profiles through markov chain modelling, Euro-Asian J. Sustain. Energy Dev. Policy 3 (2010) 12.
[90] A.C. Miller III, T.R. Rice, Discrete approximations of probability distributions, Manag. Sci. 29 (3) (1983) 352–362.
[91] B.S. Borowy, Z.M. Salameh, Optimum photovoltaic array size for a hybrid wind/PV system, IEEE Trans. Energy Convers. 9 (3) (1994) 482–488.
[92] P.D. Domanski, M. Gintrowski, Alternative approaches to the prediction of electricity prices, Int. J. Energy Sect. Manag. 11 (11) (2017) 3–27.
[93] H. Jeffreys, The Theory of Probability, OUP Oxford, 1998.
[94] R. Karuppiah, M. Martín, I.E. Grossmann, A simple heuristic for reducing the number of scenarios in two-stage stochastic programming, Comput. Chem. Eng. 34 (8) (2010) 1246–1255.
[95] Totarabank–Sustainable Rural Living [Online]. Available, https://totarabank.weebly.com/ (Accessed: 23-Feb-2023).
[96] Trading Economics, New Zealand – Real Interest Rate [Online]. Available, https://tradingeconomics.com/new-zealand/real-interest-rate-percent-wb-data.html/ (Accessed: 23-Feb-2023).
[97] UVPower, LG Chem RESU 3.3 kWh [Online]. Available, https://uvpower.com.au/product/lg-chem-resu-3-3kwh/ (Accessed: 23-Feb-2023).
[98] Eaton Corporation, XLR-48 Supercapacitor, Feb. 2019, Technical Data 10510 [Online]. Available: https://datasheet.octopart.com/XLR-48R6167-R-Eaton-datasheet-130052459.pdf (Accessed: 23-Feb-2023).
[99] SP PRO AU Series – Selectronic [Online]. Available, https://www.selectronic.com.au/sppro/ (Accessed: 23-Feb-2023).
[100] S. Mohseni, A.C. Brent, D. Burmester, A. Chatterjee, Optimal sizing of an islanded micro-grid using meta-heuristic optimization algorithms considering demand-side management, in: 2018 Australasian Universities Power Engineering Conference (AUPEC), 2018, pp. 1–6.
[101] S. Mohseni, A.C. Brent, S. Kelly, W.N. Browne, D. Burmester, Strategic design optimisation of multi-energy-storage-technology micro-grids considering a two-stage game-theoretic market for demand response aggregation, Appl. Energy 287 (2021) 116563.
[102] L. Goldie-Scot, A behind the scenes take on lithium-ion battery prices [Online]. Available: https://about.bnef.com/blog/behind-scenes-take-lithium-ion-battery-prices/, Mar. 2019.
[103] O. Schmidt, S. Melchior, A. Hawkes, I. Staffell, Projecting the future levelized cost of electricity storage technologies, Joule 3 (1) (2019) 81–100.
[104] Trina Datasheet [Online]. Available: https://static.trinasolar.com/sites/default/files/EN_TSM_PD05_datasheet_B_2017_web.pdf (Accessed: 23-Feb-2023).
[105] S. Mohseni, A.C. Brent, A metaheuristic-based micro-grid sizing model with integrated arbitrage-aware multi-day battery dispatching, Sustainability 14 (19) (2022) 12941.
[106] Solar power buy-back rates [Online]. Available: https://www.mysolarquotes.co.nz/about-solar-power/residential/solar-power-buy-back-rates-nz/ (Accessed: 23-Feb-2023).
[107] Air 40 Turbine [Online]. Available, https://www.primuswindpower.com/wind-power-products/air-40-turbine/ (Accessed: 23-Feb-2023).
[108] CliFlo: New Zealand's national climate database [Online]. Available, http://cliflo.niwa.co.nz/.
[109] The Electricity Market Information, The New Zealand electricity authority's wholesale database [Online]. Available: https://www.emi.ea.govt.nz/Wholesale/Reports/.
[110] B. Anderson, NZ GREEN grid household electricity demand data: EECA data analysis (part C) upscaling advice report v1.0, Available: https://ourarchive.otago.ac.nz/handle/10523/9820, 2019.
[111] D.E. Goldberg, J.H. Holland, Genetic algorithms and machine learning, Mach. Learn. 3 (1988) 95–99.
[112] J. Kennedy, R. Eberhart, Particle swarm optimization, in: Proceedings of ICNN'95-International Conference on Neural Networks vol. 4, 1995, pp. 1942–1948.
[113] L. Urbanucci, D. Testi, Optimal integrated sizing and operation of a CHP system with Monte Carlo risk analysis for long-term uncertainty in energy demands, Energy Convers. Manag. 157 (2017) (2018) 307–316.
[114] E. Leo, S. Engell, Multi-stage integrated electricity procurement and production scheduling, in: M.R. Eden, M.G. Ierapetritou, G.P.B.T.-C.A.C.E. Towler (Eds.), 13 International Symposium on Process Systems Engineering (PSE 2018) vol. 44, 2018, pp. 1291–1296.
[115] S. Mohseni, A.C. Brent, D. Burmester, Community resilience-oriented optimal micro-grid capacity expansion planning: the case of Totarabank Eco-Village, New Zealand, Energies 13 (15) (2020) 3970.
[116] Electricity Authority, Investigation into the value of lost load in New Zealand – report on methodology and key findings [Online]. Available: https://www.ea.govt.nz/assets/dms-assets/15/15385VOLL-technical-report.pdf, 2013 (Accessed: 23-Feb-2023).